INFORMATION TO USERS

This manuscript has been reproduced from the microfilm master. UMI films the text directly from the original or copy submitted. Thus, some thesis and dissertation copies are in typewriter face, while others may be from any type of computer printer.

The quality of this reproduction is dependent upon the quality of the copy submitted. Broken or indistinct print, colored or poor quality illustrations and photographs, print bleedthrough, substandard margins, and improper alignment can adversely affect reproduction.

In the unlikely event that the author did not send UMI a complete manuscript and there are missing pages, these will be noted. Also, if unauthorized copyright material had to be removed, a note will indicate the deletion.

Oversize materials (e.g., maps, drawings, charts) are reproduced by sectioning the original, beginning at the upper left-hand corner and continuing from left to right in equal sections with small overlaps.

Photographs included in the original manuscript have been reproduced xerographically in this copy. Higher quality 6" x 9" black and white photographic prints are available for any photographs or illustrations appearing in this copy for an additional charge. Contact UMI directly to order.

Bell & Howell Information and Learning
300 North Zeeb Road, Ann Arbor, MI 48106-1346 USA
800-521-0600

ACQUISITION AND ANALYSIS OF CUTTING FORCES OF SURGICAL INSTRUMENTS FOR HAPTIC SIMULATION

Stephanie Greenish

Department of Electrical and Computer Engineering
McGill University

October 1998

A Thesis submitted to the Faculty of Graduate Studies and Research
in partial fulfilment of the requirements for the degree of
Master of Engineering

Abstract

Current research has focused on visual feedback for the development of virtual surgery. However, little is known about the haptic feedback required for realistic simulation. The forces necessary for the cutting of anatomical tissues were investigated for three surgical scissors: the Mayo dissection scissor, the Metzenbaum dissection scissor and the Iris scissor. Several experiments were completed in conjunction with a surgical doctor to acquire force data for analysis. This work aimed to establish the force-position relationship, find any invariant properties for tissues or scissors, and determine the frequency components present in the force signal as well as the significance of the cutting rate. General trends in the data were discovered, and necessary improvements to the experimental method for the determination of more exact quantitative measures were identified.

In general, both the measurable force magnitude and "texture" differences contribute to the difference in tactile perception between a blank run and a tissue cutting run. This is a low frequency texture, as 99% of the frequency components of the signal are below 5Hz. The force measurements were determined to be independent of the cutting speed for the Mayo and Metzenbaum scissor runs, whereas results for the Iris scissors were inconclusive. The scissor sensitivity while cutting the tissue longitudinally or transversally appears to be a function of both the tissue and the scissor. To further determine the tactile feedback required for simulation, future experiments should account for the "user grip", tissue thickness, tissue moisture content, hand orientation, and innate scissor dynamics.

A database of the collected force and position data has been created on the Internet (Site:http://www.cim.mcgill.ca/~haptic/tissue/data.html). This data allows current force feedback devices, such as the Freedom-7, to determine the feasibility of realistic haptic simulation.

Acknowledgements

This work is a direct result of the contributions of my supervisors Vincent Hayward and Dr. Thomas Steffen. Thank you for your ideas and support.

As well, there are many people who have generously given their help. Thank you George Dedic and George Tewfik for all of the support and technical expertise you kindly offered. I might still be working on those strain gauges now if not for your help. Thanks to Don Pavlasek for the impeccable machining and instruction regarding the scissors. Thank you Phil Downer and Hani Baramki for your help during experimentation, especially for the tissue preparations.

A special thanks goes to Danny Grant, Oliver Astley, Michel Doyon and Manuel Cruz for their many ideas and advice. You have been great office mates and your numerous contributions are greatly appreciated. Thank you Michael Greenish and Linda Rauch for the moral support and encouragement and naturally, thanks to my parents who have been in my corner all along. I really appreciate all that you have done for me.

Finally, I would like to thank the Natural Sciences and Engineering Research Council for their financial support.

TABLE OF CONTENTS

LIST OF FIGURES

LIST OF TABLES

CHAPTER 1

Introduction

1. Virtual Surgery

Virtual surgery, or virtual reality technology in the field of surgery, holds many promising possibilities. Among its many applications, virtual surgery could train new surgeons in a virtual environment, without the expensive and time-consuming burden of using cadavers. As well, students could repeat, as often as necessary, complicated surgical procedures without increasing the cadaver count for each trial. Beyond teaching new techniques, the virtual environment could help prepare students for the fast-pace of the emergency room where a doctor must adapt efficiently to a constantly changing environment. Its usefulness would not be limited to training new surgeons however. It would permit experienced surgeons to practice new techniques and accommodate a brush-up for rarely used techniques, in a short period of time, thereby reducing the chance of human error. Furthermore, it could enable the planning and trial of completely new surgical techniques which have never been performed. With accurate tissue models, the recovery for a new procedure could be simulated and monitored, thereby establishing a realistic prediction method for the efficacy of new procedures.

In the same way flight simulators today account for most of the training hours for commercial pilots, surgical simulators will one day become an integral part of training for surgeons around the world. This will inevitably dictate a standardisation of procedures and thereby establish quantifiable metrics of performance, which will provide an objective assessment of a new surgeon's capabilities. All of this, before a real incision is ever executed.

The applications of virtual surgery can be grouped into four main fields of current research: teaching, training, predicting the outcome of operations, and planning and performing surgical operations.

For a realistic virtual environment (VE), the senses of sight, sound, smell and touch need to be reproduced; taste is insignificant for most applications. According to Faulkner [9], the senses, upon receiving stimuli from their environment, process the information in parallel, using different percentages of the available human bandwidth: 70% for vision, 20 % for audition, 5% for olfaction and 4% for cutaneous. Because the visual system plays such an important role in a simulation, most work has been focused on developing the software for a realistic visual environment. However, the visual environment is not sufficient for realism. As Rosen points out in [23], there are five distinct areas necessary for realism in a surgical simulation: (1) good fidelity, enough high resolution in the image for it to appear real, (2) good object properties, the organs must deform as expected when grasped and released, (3) good reactivity, the organs must react to manipulations properly like bleeding upon cutting, (4) good interactivity, the interaction of the surgeon's instrument and the organs must be realistic, and (5) good sensory input, which includes force feedback, tactile input and pressure felt by the surgeon.

Thus, for a realistic virtual surgery, tactile feedback, or haptics, is a necessary part of this realism. Naturally, the trade-off for greater realism is more computational power and hardware.

2. Objectives

This work investigates the forces experienced by a surgeon while cutting different tissues, allowing a broadening of the knowledge of what haptics must be reproduced to achieve realistic force feedback during virtual surgery. Although there has been a substantial amount of research in the static properties of tissues, the dynamic relationships remain relatively unknown [6] [10]. For this reason, the first objective of this work was to acquire the force data for the dynamic manipulation of biological tissues. Experiments were performed with three surgical scissors, the Mayo dissection scissor, the Metzenbaum dissection scissor and the Iris scissor, see Appendix A.

Once the data were acquired, the analysis aimed to answer the following questions: (1) Is there a quantifiable force difference between different tissues? (2) What frequency components are present in the signal and what knowledge about the sensory feeling do these provide? (3) Is the force measured invariant to the velocity? and (4) Are there any other invariant properties of the tissues or of the scissors which can be determined?

In order to achieve these results, Dr. Thomas Steffen, Director of the Orthopaedic Research Laboratory at the Royal Victoria Hospital and Assistant Professor of Surgery at McGill University, provided co-supervision and helped realize several animal experiments at approved McGill animal-care facilities. All experiments were done on animals which had

been sacrificed for other research and in accordance with animal protection laws. Thanks to Dr. Steffen, three separate experiments with animals were realized. These experiments involved the cutting of the animal tissues with the instrumented scissors. Since these were planned sacrifices, it was possible to perform the experiments immediately after death. It was therefore unlikely that post-mortem changes had occurred, which are known to alter the mechanical properties of tissues considerably [6].

As an end goal, this work will supply the knowledge of the forces involved in the cutting of tissues, so that these forces can be applied by the Freedom-7 Hand Controller [14], to provide force feedback in a surgical simulation. The Freedom-7 is described in more detail in Chapter 2.

3. Overview

Chapter 2 provides a review of the advances made toward virtual surgery, as well as a background in the haptics involved. The data acquisition set-up, experimental apparatus and sensor calibration are described in Chapter 3. The data analysis performed to answer some of the proposed thesis questions is presented in Chapter 4. Section 1 investigates the measurable differences that exist between tissue types and identifies general trends in the force data. Section 2 explores the frequency components in the signals to understand what components in the signal need to be reproduced by a simulator, as well as, what creates the differences in feeling between tissues. The contribution of velocity to the force information is analysed in section 3 and the tissue and/or scissor invariants are explored in section 4. Finally, the conclusions are presented in Chapter 5.

CHAPTER 2

Background

1. Current Developments

Virtual surgery furthers the connection between engineering and medicine. This bridge is being made in many different fields which include research in model development for such things as human tissues, bones and organs, as well as the development of hardware and software which help doctors "see" inside patients either for diagnosis or treatment. The meeting of the two fields provides a deepening of the understanding of both medicine and engineering. Several advances have been accomplished which continually facilitate the conceptualisation of a completely virtual environment for surgery.

1.1. Telesurgery. Teleoperation is defined as "the extension of human inspection and manipulation capability to remote or otherwise inaccessible locations" [27]. The device which provides communication to and from the human operator, and allows for this inspection through sensors and actuators, is termed the teleoperator. From these concepts naturally developed "telesurgery". In telesurgery, the actual surgery is occurring at some distance from the surgeon. It is this distance which engineering strives to narrow.

Telescopy is a primitive form of telesurgery where the surgeon is remote from the surgery because the operation is performed through small holes. This renders the operation site invisible to the surgeon. Endoscopic surgery, a form of telescopy, is a minimally invasive surgery (MIS) which allows percutaneous operation on a particular region of interest within the body through small incisions. The endoscope provides images of the surgical site to the surgeon on a monitor which allows the surgeon to see what is happening. Current endoscopic methods include arteriography (coronary arteries), thoracoscopy (the chest), laparoscopy (the abdomen), arthroscopy (joints), and gastroscopy (gastrointestinal tract) [7]. There are many advantages to MIS techniques including shorter recovery times, lower risk of bacterial infections, local versus general anaesthesia and smaller visible scars. However,

the instruments are harder to use because they are awkward and provide little sensory (tactile, force, pressure) feedback. Continuing research is being done to improve these MIS instruments by making them smaller, increasing their dexterity and increasing the amount of sensory feedback provided [2, 23].

Another form of telesurgery is microsurgery where, although the surgeon is not operating through small tubes, the surgeon is remote (tele) in the sense that the surgical task is very small, as for example in eye surgery [27]. In these instances, a charge-coupled device (CCD) camera and video display are used to enlarge the work area, enhancing the surgeon's ability to see the structures being operated on.

These two types of telesurgery involve having the patient and surgeon physically near one another. A third type of telesurgery involves an unavoidable large distance between the surgeon and patient. This is often referred to as telemedicine. The advances in telemedicine have been mainly diagnostic thus far, for example reading x-rays at a remote medical centre or mentoring local physicians [12]. Philip Green, a pioneer in telepresence surgery, envisions that in the future, "telepresence will enable expert surgeons to actually participate in surgeries at local clinics." Although current technology is still far from this, the field of knowledge is expanding.

1.2. Telepresence Surgery System. Advances realized in telesurgery include the Green Telepresence Surgery System developed at SRI International by Philip Green. The system, described in [13], consists of two main modules: a surgeon's console where the surgeon operates in a virtual space and a remote surgeon's unit which performs operations on a patient. It was designed for three applications: telesurgery, minimally invasive surgery (especially laparoscopic) and microsurgery. SRI has developed a battle field version to provide surgical services in dangerous environments and has named it the *medical emergency forward area surgical telepresence* (MEDFAST) [24, 26]. In this version, a surgeon operates in a virtual space at a console and the motions are translated by a slave robot to a patient lying in the MEDFAST. An essential advantage of the Green Telepresence Surgery System is its versatility to adapt to different functions. With a simple operation like a change of scale, it can change from operations such as endoscopy to microsurgery [16].

Other important research in the development of surgical simulators is the work of Delp, Rosen and associates of MusculoGraphics, Inc. and MedicalMedia, Inc., who are developing the anatomical rendering, tissue interactions and surgical instruments for a specific surgical instance, a gunshot wound in the thigh. Recently, Delp et al. [5] presented their 3-dimensional, interactive computer model of the human thigh which was constructed from the data provided by the Visible Human Project [1]. Similarly, Merrill, Higgins and

colleagues of High Techsplanations, Inc. are developing the anatomic rendering, tissue interactions and surgical instrumentation for a shattered kidney [25]. Eisler of Mission Research Corp. is working in tissue damage as a result of a ballistic wound for which Cuschieri from the University of Dundee is supplying basic tissue properties [25].

1.3. Computer-Assisted Surgery. Another field of research where engineering and medicine meet is in computer-assisted, or augmented-reality, surgery. This is an integration between available medical data acquisition units and a robot. Examples of the medical data acquired include pre-operative images (CT Scans, MRI, Angio-MRI, SPECT, TEP, MEG, Stereo-Angiograms...), anatomical models, intra-operative images (X-rays, ultrasound images, video images), position information, shape information and coordinate systems [8].

The ROBODOC is one such device. The initial application of the ROBODOC was for total-hip replacement, or anthroplasty, where the robot prepares a cavity in the femur, making room for an artificial implant. With the use of CT Scan images, a pre-operative milling tool path is created in a 3-dimensional reconstruction of the femur which the ROBODOC can then mill with high precision [17]. Another augmented reality device is the MINERVA robot, developed by the Swiss Federal Institute of Technology [3,11]. The MINERVA helps surgeons perform stereotactic brain surgery where surgeons perform surgery by inserting instrument probes through a small hole in the skull. When operating in this manner, surgeons have the advantage of minimal brain shifting resulting from liquid displacement, but the disadvantage of not having the brain visible. By designing the robot such that it fits within a CT Scanner and having the patient fixed in a Brown-Roberts-Wells (BRW) frame, the robot is capable of various autonomous tasks including: making skin incisions, drilling the cranium, perforating the meninges and manipulating stereotactic instruments. There has also been research in knee surgery [31], mediastinoscopy and retroperitoneoscopy [2] and many other applications of augmented-reality robots.

The field of virtual surgery is growing and applications for linking engineering and medicine only expanding. However, there are many advances to be made and many challenges to be overcome before a completely integrated virtual surgery system exists.

2. Haptics

Realism in a virtual simulation is increased multiplicatively with each additional sense. At present, most systems do not have a good integration of the tactile feedback. This is largely explained by the complexity in adding realistic haptics due to hardware limitations. Systems which can display high forces typically have a small workspace and systems with a

large workspace are typically limited in their abilities to display sufficiently high forces for realism.

Creating virtual haptic feedback for an environment that is to resemble the real world requires an algorithm which parameterises in some way the physical environment. There are several ways of obtaining such an algorithm. One method is to take a purely perceptual approach where the model is based on what feels right and this determines how the final parameters are chosen. Although this approach achieves good fidelity, it is highly subjective and, therefore, not highly repeatable among different users. As well, due to its iterative nature, it is time consuming. Another method is to take a purely structural approach, where each aspect of the physical environment is dissociated and modelled with friction coefficients, spring constants and other such physical properties. Although this method provides a very repeatable result that is based on the physical environment, it is difficult to ensure that all key components have been modelled. A third method, a "black box" approach, measures the output of the system for controlled inputs. MacLean [20] calls this the "Haptic Camera." The advantages of this type of active probe include the objectivity of parameterising the system and repeatability. Naturally, the best algorithm is obtained when all of the above three methods are combined. A knowledge of the underlying mechanical structure provides a good understanding of which inputs and outputs must be measured. Once an algorithm is found, it is good to then have an iterative final approach which fine tunes the parameters for realism.

It is important to keep in mind, however, the findings of Srinivasan [28] that the perception of stiffness is greatly influenced by visual information. His experiments have shown that the visual information can fool a user receiving conflicting haptic and visual inputs. This suggests that a good visual representation can overcome some of the limitations of poor haptic feedback. This is an important result since, as mentioned previously, most haptic devices are incapable of displaying the range, resolution and frequency bandwidth of forces that the human is able to perceive tactually.

3. Instrument Selection

One of the first steps of this work involved a familiarisation with surgical instruments. One thing which became evident early on was that, among the thousands of surgical instruments that exist for thousands of very specialised tasks, there are only a limited number of basic handle designs to interface with the surgeon's hand. The most popular handle types are the scissor handle, the knife end, the tweezer, or dissection forcep, and the hemostat, or artery forcep, see Figure 2.1.

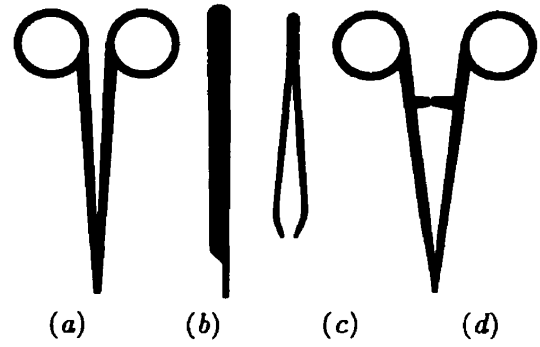

FIGURE 2.1. Basic handle types: (*a*) the scissor handle, (*b*) the scalpel, (*c*) the tissue forcep, (*d*) the hemostatic forcep.

From these four basic handle types, many variations exist. For example, for scissors the arm lengths vary from 2″ (5.1 cm) to over 10″ (25.4 cm), the breadth of the arms varies from less than an $\frac{1}{8}$″ (0.3 cm) to over $\frac{1}{4}$″ (0.6 cm), and the tip specifications change, all depending on the application. The various tip structures available include: with teeth or without, curved or straight, pointed or blunt. Furthermore, the blades can be sharp or dull, tight or loose depending on the joint screw and each of these factors influence the "feel" of the scissor. From a simulation point of view with a programmable device such as the Freedom-7, this diversity is not a grave problem, since many of these features can be simulated.

3.1. Basic Dissection Set. The first set of surgical instruments investigated was a basic dissection set, as that is one of the first tasks learned in medical school. From [29], it was learned that this set includes over 20 different types of instruments, see Appendix A.

The initial idea was to have a complete set of instruments to be able to perform one integral task, which could then be simulated in its entirety. As is pointed out in [25], an integration of the three environments (pre-, inter-, and postoperative) is required for realism, hence a complete set is needed. However, a problem of feasibility was quickly encountered and the basic set had to be reduced for this work.

In the basic dissection set, there are many retractors which serve only to expose the wound. These were the first instruments eliminated from the test set. The second group of instrument to be eliminated from the set were any which required a closing force too large to reproduce virtually, for example most of the hemostats. It was assumed that, any instrument which requires such a high force to close would not be modelled virtually, but rather would be integrated into the design of the end-effector, or end piece of the robotic device which interfaces with the user's hand. For example, the hemostatic forcep handle shown in Figure 2.1*d* serves as a good robot end-effector to interface with the user's hand

and the blade-end feedback would then be provided virtually. Therefore, leaving the ratchet of a hemostat in the real world, rather than trying to make it virtual, poses itself as a good solution to the problem of limited force capabilities of most simulators discussed earlier. Furthermore, since hemostats are used mainly to hold and pull small tissues such as veins, only the resistance of the ratchet is felt when closing. That is to say, the force feedback involved in the closing down on these tissues is negligible. Therefore, the haptic problem with respect to the hemostats is reduced to simulating the pulling of tissues which would be rendered virtually.

3.2. Preliminary Experiments. After eliminating all instruments which were not feasible or not interesting from a force simulation point of view, five instruments remained in the subset: a Metzenbaum dissection scissor, an Adson tissue forcep, a Wescott micro-scissors, a Halstead mosquito hemostatic forceps and a Bard Parker knife. These can be seen in Figure 2.2. Although the basic dissection set does not include a micro-scissor, it

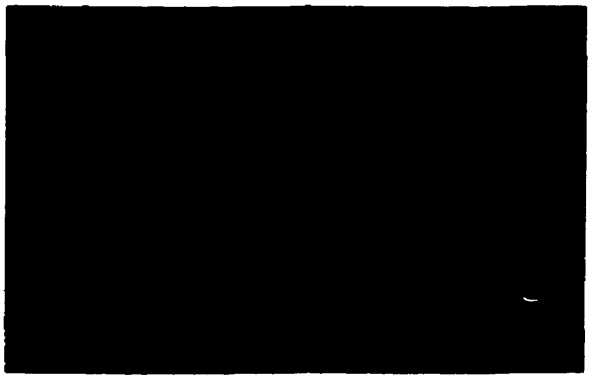

FIGURE 2.2. From left to right, Metzenbaum dissection scissors (7" (17.8 cm), straight), Adson tissue forceps (1 x 2), Wescott micro-scissors (blunt-blt, 11cm), Halstead mosquito hemostatic forceps and a Bard Parker knife (No 3).

was also purchased for investigation. The first set of experiments were performed at the Royal Victoria Hospital using these instruments upon a dog. Several problems of the data acquisition system were identified immediately.

The device used to measure the position in 3-space had a workspace which was far too limited. It was initially thought that the work space of any operation would be relatively small, but this is not entirely true. The work space is small only after a relatively large tissue area has been prepared. Since the instruments purchased are mainly used for the preparation of a surgical work space, the freedom to move in a large work volume was imperative. Furthermore, the depth of reach requirements were larger than predicted and the doctor was unable to cut the tissues while hooked up to the position sensor.

Although the dog was of moderate size, finding appropriate tissues for cutting required a fair amount of preparation. In all, the upper and lower abdominal areas and the hind leg were used. Each region change required moving the entire position sensor which was time consuming and inconvenient as the restrictions of post-mortem effects become relevant.

In brief, from this first set of experiments, it was discovered that all of the instruments, with the exception of the scissors, have a pronounced need for simultaneous spatial data to be collected in conjunction with the force data. The reason scissors are exempt from this requirement is that their opening angle contains most of the position data necessary. By measuring the scissor angle, the only event which is indeterminate is when the contact is made between the scissor and the tissue. Once the contact is made, the opening angle determines the position. This type of position data, however, is not readily available for the knife, which is typically used to make a large incision, nor for forceps, which are used to pull tissues or vessels. Thus, for this work, it was decided to focus on surgical scissors. The other instruments remain for future work.

Since it was learned from working with Dr. Steffen that surgeons typically prefer a curved tip, which allows clearer visibility of the work area, a new scissors were purchased and equipped with instrumentation. This second set consisted of: a 7" (17.8 cm) Metzenbaum scissor with tungsten carbide inserts, a $6\frac{3}{4}$" (17.1 cm) Mayo scissor with tungsten carbide inserts and a pair of $4\frac{1}{2}$" (11.4 cm) Iris scissors, all with curved tips. The Mayo and Metzenbaum were selected since they are in the basic dissection set. Although not part of the dissection set, the small Iris scissors were purchased for comparison since the other two scissors are of medium size.

The dog experiment helped set the protocol for later experiments. For skin, the abdominal area was determined to be the best since it provides a relatively large area of skin which is uniform. Furthermore, preparing the abdominal area serves the dual purpose of exposing several other tissue layers just below the skin, which in turn implies shorter tissue preparation times. Naturally, the element of time is important since post-mortem for an animal the size of a dog sets in within roughly two hours. The doctor deemed it preferable to leave the internal organs such as the stomach, large intestines, small intestine and bladder undisturbed for clean-up and odour reasons.

3.3. Freedom-7 Hand Controller. As an end goal, the forces obtained from this research will serve to provide force feedback with the Freedom-7. The Freedom-7 is a high fidelity, seven axis haptic device which has a 3 degree-of-freedom (DOF) positioning stage and a 4-DOF orientation stage, see Figure 2.3 [14]. The seventh degree is well suited to mimic a pinching or closing action, like that of a scissor, forcep or hemostat.

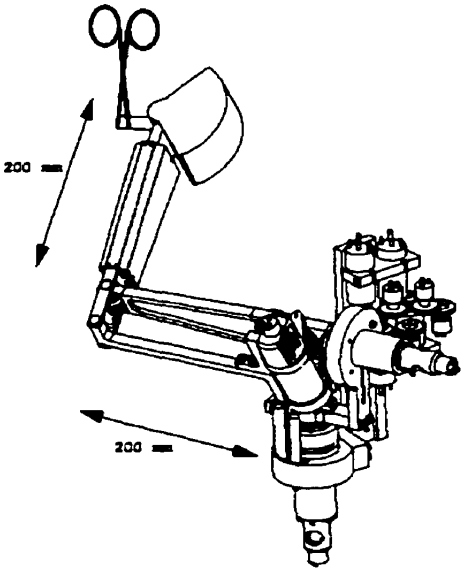

FIGURE 2.3. Freedom-7 shown without its holding stand and with a scissor end-effector.

In order to use the Freedom-7 for the playback of surgical scissors, end-effectors for the hand controller are required which imitates these instruments. Since there are many different dimensions for these instruments, as was described in detail for the scissors, the number of end-effectors required quickly becomes infeasible. In order to reduce this to a manageable number, one end-effector must simulate as many instruments as possible.

4. Sense of Touch and Feeling

A brief description of skin is provided in Appendix B. Essentially, there is a distinction to be made between the sense of touch and resolved force feedback. In the human body, Golgi and other receptors mediate the sensation of force, whereas those in the skin (Meissner, Merkel, Pacinian and Ruffini sensors) mediate touch. Touch exhibits a differential sensitivity of about 1 mm in the plane of the skin surface [27]. Resolved force magnitude sensitivity, however, exhibits a much smaller differential threshold and operates over a much larger force range. In this application, it is resolved force feedback which is important as the sense of touch will be reproduced by the physical presence of surgical end-effectors.

CHAPTER 3

Data Aquisition

1. Sensors

In order to determine the forces that the surgeon experiences during cutting, the scissors were equipped with sensors. Strain gauges were used to measure the force, and precision potentiometers were used to measure the angle.

1.1. Force Measurement.

1.1.1. *The Force Sensor.* A strain gauge is a resistor whose resistance changes as the gauge length changes, i.e. when the gauge is stretched or compressed. As the scissor cuts through a material, the scissor arm bends slightly and it is this bend which compresses or stretches the gauge. It is in this manner that the force applied by the tissue being cut is measured.

Plastic behaving materials, like stainless steel scissors, exhibit a typical stress-strain behaviour. This can be modelled as a combination of elastic behaviour and a limiting yield stress σ_y, after which increasing the strain will not increase the stress [32]. This model is shown in Figure 3.1*a*. However, since most materials do not behave in this ideal manner,

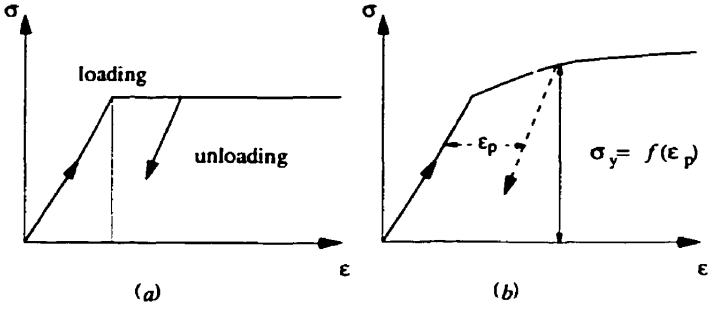

FIGURE 3.1. Uniaxial stress-strain behaviour: (*a*) Ideal plasticity. (*b*) Strain hardening plasticity.

a refined model exists. It is based on the hardening and softening of the plastic material and therefore has a σ_y which is a function of the plastic strain, ε_p (Figure 3.1*b*). Since the scissors were not used to cut hard material such as bone, all strains experienced were in the elastic range and therefore, the simplified model can be used.

To measure the force, two different types of strain gauges were tried, foil and semiconductor. The first set of experiments were performed with the foil type resistors of which two versions were used, the MicroMeasurement SK-06-S065R-10C (1000 Ω resistor) shown in Figure 3.2*a* and the MicroMeasurement SK-06-062TW-350 (350 Ω resistor) shown in Figure 3.2*b*. Subsequent experiments were performed with semiconductor Entran ESU-025-1000 gauges as shown in Figure 3.2*c*.

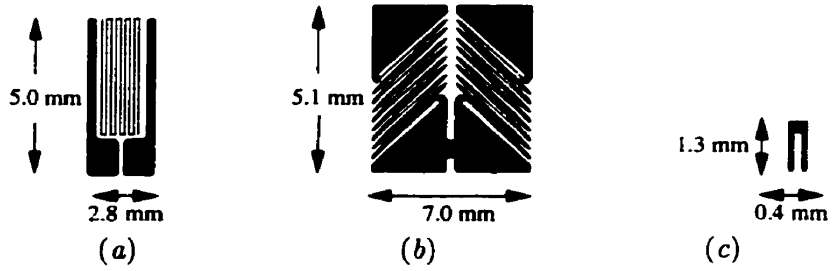

FIGURE 3.2. Foil type strain gauges: (*a*) SK-06-S065R-10C and (*b*) SK-06-062TW-350. Semiconductor type strain gauge: (*c*) ESU-025-1000

In the first experiments, the gauges in Figure 3.2*a* were mounted length-wise in a half-bridge configuration on the top and bottom side of one arm. This direction is indicated in Figure 3.3*a*. In this manner, one gauge is being compressed as the other is expanding. Naturally, the gauges were placed near the centre of the arm to take advantage of the maximum bending. The 45° gauges, Figure 3.2*b*, were mounted on the sides of the scissor arm with the resistor foil directions matching the arrows in Figure 3.3*b*. This actually gave a full bridge since each strain gauge consists of two resistors.

The advantage of using the 1000 Ω resistors is a larger raw signal. The disadvantage is their higher sensitivity to noise compared to the 350 Ω resistor. However, it was found from preliminary runs that, at the level of signal obtained, the increase in the amount of noise was less than the increase in the amount of signal. Similarly, it was found that the 45° gauges are not sensitive enough in the manner that they were installed, on the side of the scissor arm. The gauges experience much more expansion and compression when placed in the axis of the arm, as in Figure 3.3*a*, and therefore this mounting arrangement was employed for the second set of experiments with the semiconductor gauges.

The shift to semiconductor gauges was made after the preliminary dog runs because, due to limited availability, the signal conditioner unit was changed. The new unit required

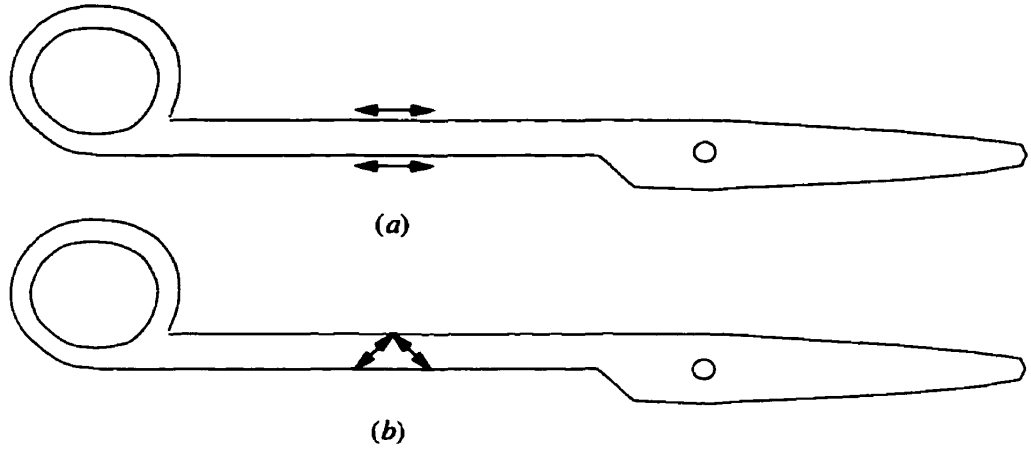

FIGURE 3.3. Directions and positions of strain gauge mountings: (*a*) along the scissor axis and (*b*) 45° to the axis.

a higher input signal to noise ratio (SNR). The Entran ESU-025-1000 U-shaped gauges (see Figure 3.2*c*) were used which have a nominal gauge factor (GF) of +155 where

$$GF = \frac{\delta R/R}{\delta L/L} \pm 5\% \tag{3.1}$$

where R is the resistance, δR is the change in resistance, L is the length of the gauge and δL is the change in length. When compared to foil type gauges, which typically have a GF of +2, the semiconductor gauges give approximately 75 times more signal. Their drawback is the increased complexity in mounting (see Mounting Instructions in Appendix C). Briefly, the gauges are much smaller and cannot be touched by hand. They must be handled with fine tweezers by their delicate gold leads which are prone to breaking during gluing and prone to evaporation during soldering. Some recommendations for their application can be found in Appendix C.

1.1.2. *Signal Acquisition and Conditioning.* All strain gauges were excited and read with a signal conditioner. For the initial dog experiments, a 2100 Strain Gauge Conditioner and Amplifier System from Measurements Group, Inc. was used with a sampling speed of 700 Hz. However, since this system was unavailable for future experiments, the conditioner used for the sheep and rat experiments was the Analog Devices 3B Series Signal Conditioning I/O Subsystem[1], with the 3B01 16-channel backplane and Model 3B18 Wideband strain gauge input modules. The 3B18 accepts strain gauge inputs and provides bridge excitation of ±10 volts. The bandwidth of the module is 20 kHz. The sampling speed used was 1000 Hz. A functional block diagram for the 3B18 is shown in Figure 3.4.

[1]If affordable, the 2100 System Strain Gauge Conditioner and Amplifier System from Measurements Group, Inc. is much better suited to these types of measurements.

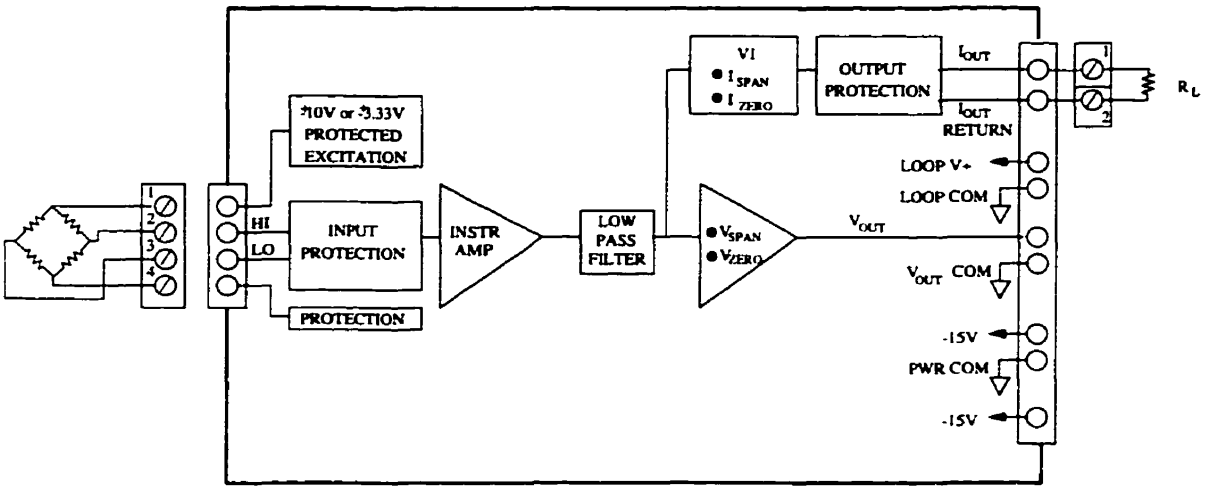

FIGURE 3.4. Functional Block Diagram of 3B18 Input Modules for the Signal Conditioner

Since the 3B18 does not allow for internal bridge balancing, an external bridge balance was constructed as shown in Figure 3.5 [30]. The zeroing potentiometer used had a resistance of 10 kΩ. The sensitivity potentiometer was omitted because it decreases the measured voltage and thereby decreases the signal power. R_1 and R_2 are the semiconductor strain gauges where one branch is in compression and the other is in expansion. R_3 and R_4 are bridge-completion (dummy) resistors in the case of the half-bridge configuration. For these experiments, R_3 and R_4 were provided by a bridge completion module from MicroMeasurement, module MR1-10C-129.

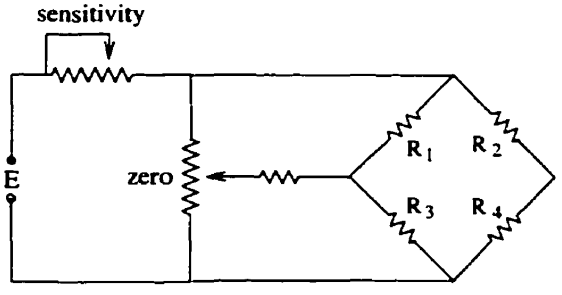

FIGURE 3.5. External bridge balancing circuit

1.2. Angle Measurement. The angle was measured with a $\frac{1}{4}$-turn rotary precision potentiometer (pot). More specifically, Midori "blue-pot" contactless potentiometers were used (model CP-2UTX). These pots were selected for their high resolution, stability and low friction. A special fixture was machined which allowed the mounting of the pots without any modifications to the scissors themselves, avoiding changes in the scissor dynamics. A

bracket arm was made for each of the scissors to hold the pots in position. A sleeve, with a set-screw which clamps down on the shaft of the potentiometer at one end and a blade at the other, was used to couple the shaft of the pot to the joint screw, see Figure 3.6. Although these fixtures were bulky, the potentiometers were placed such that they were pointing up and away from the operation site. The system was designed to be rinsable after an operation, so all seals were covered with silicon.

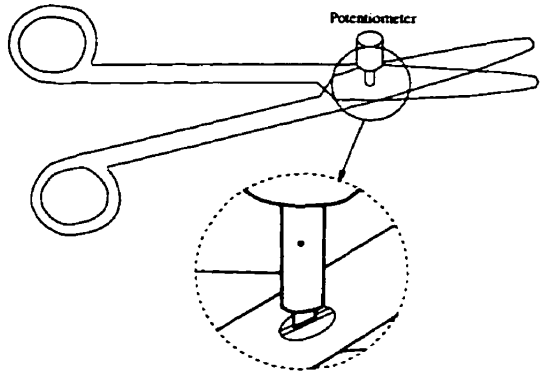

FIGURE 3.6. Mounting of the potentiometer used to measure the angle during cutting.

The signals from the potentiometers had good SNRs, therefore no conditioning was necessary.

1.3. Experimental System. A block diagram of the system is presented in Figure 3.7. In the top left-hand corner are the strain gauges as described in Chapter 3 section 1.1.1. The bridge completion and zeroing stage was described in Chapter 3 section 1.1.2. Although the amplifiers and filters have been shown as a separate stage, they are actually integrated in the signal conditioner unit (see Figure 3.4). The computer used was a 167 MHz Pentium by Ultinet.

Furthermore, the analog-to-digital (A/D) conversion step is shown as outside of the computer, however an internal PC board was used to perform the A/D and D/A conversions. The board was a Real Time Devices ADA1110 board which provided 12-bits resolution at 20μsecond conversion with 40 kHz throughput. The DACs (digital-to-analog converters) were used to provide +10 volts excitation to the potentiometers and the ADCs (analog-to-digital converters) read the signal from both the potentiometers and the strain gauges. For the voltage ranges used, the position and force measurements were quantised to $\sim$ 0.005 V resolution.

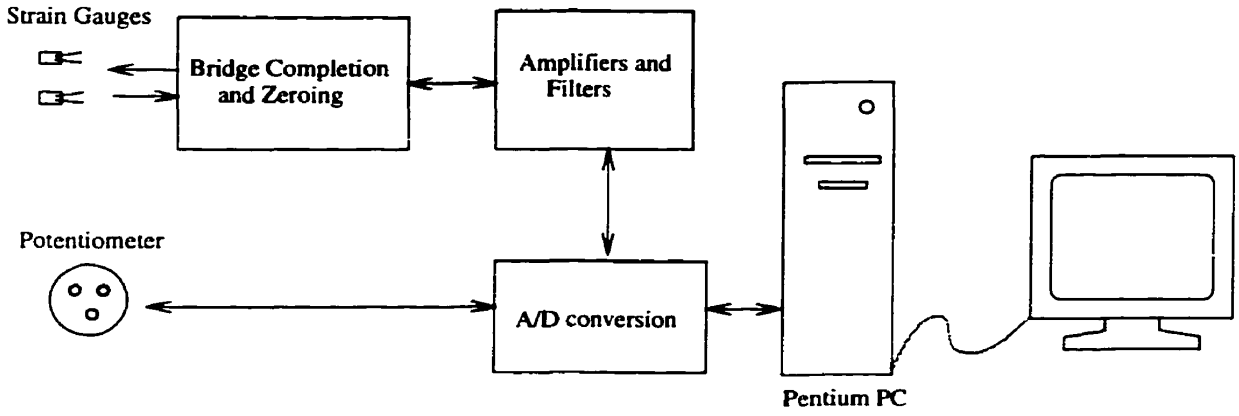

FIGURE 3.7. Block diagram of data acquisition set-up.

2. QNX

The QNX™ Operating System was used to handle the data acquisition of the force and position data since it is highly suitable for real-time applications. It is in essence a UNIX™ Operating System for a PC. In order to have a fast visual feedback of the state of the system, a graphical user interface (GUI) was designed and implemented in Photon, a graphical user interface environment for the QNX™ real-time operating system.

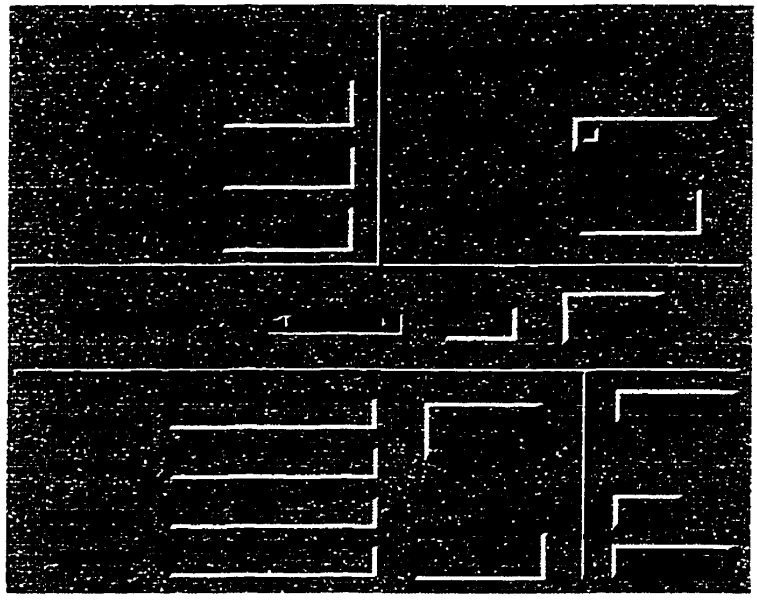

FIGURE 3.8. Graphical user interface made in Photon to control data acquisition.

2.1. Graphical Interface. The GUI allows for a visual display of force readings and angle readings as the measurements are being read, see Figure 3.8. This permitted a quick visual assessment of the system, as well as, facilitated control of the data acquisition and storage.

The read-outs for each of the three scissors can be found in the upper left-hand corner. The GUI was set up to continuously monitor the 3 scissors. In the upper right-hand corner, the power supplied to the potentiometers is controlled and the response is displayed. The toggle buttons change from grey to green when +10 V DC is supplied to the potentiometers.

The scroll bar allows the sampling frequency to be changed rapidly. The data storage is controlled in the lower left-hand corner. Any information entered into the data entry blocks, such as the user name, instrument type or comments, appear in the output file as a comment. As well, the data files are time stamped.

3. Calibration of Force Sensor

To convert the strain gauge readout from volts to a meaningful force measure, it was necessary to analyse the scissor dynamics. During a cutting act, the $\overline{OF}$ distance in Figure 3.9 remains constant whereas the $\overline{OC}$ distance varies, where C is the point of contact of the two scissor blades and incidently where it is assumed the cutting is taking place.

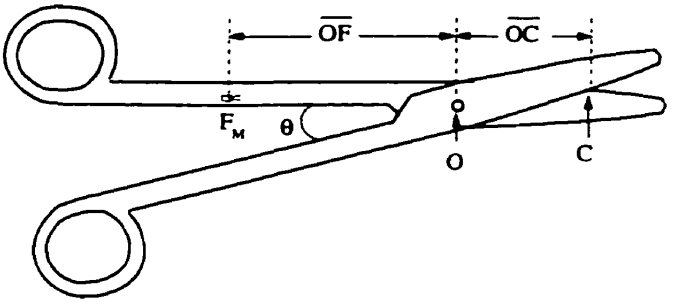

FIGURE 3.9. Scissors where $\overline{OC}$ is the cutting distance and $\overline{OF}$ is the distance from the focal point to the force measuring sensor.

Since the lever arm is changing, the same handle force applied while at a position C_1 (distance $\overline{OC_1}$ along the blade) will read differently than if the contact point is at a position C_2 (distance $\overline{OC_2}$). However, since the force measurement and angle are known simultaneously, the angle position can be used to calculate the true handle force applied, as well as the true force applied at C.

Starting with the simple balance equation for the forces, one obtains

$$F_M\overline{OF} = F_C\overline{OC} \tag{3.2}$$

where F_C is the force applied at C. It is hard to measure F_C however, when the scissors are free floating as in Figure 3.9, so the calibration of the scissors was accomplished using a force transducer (calibrated load cell) and indicator, see Figure 3.10. The load cell provides a measure for F_C in Newtons. For Equation 3.2 to hold, both F_C and F_M must have the same units, therefore the F_M is also needed in Newtons. Therefore, F_M is replaced by F_M/k, where k is a constant with units of V/N and is a function of the signal conditioner gain and scissor characteristics. This gives the relationship

$$F_M\overline{OF} = kF_C\overline{OC}, \tag{3.3}$$

which can be rearranged to give,

$$k = \frac{F_M\overline{OF}}{F_C\overline{OC}} \tag{3.4}$$

where k is determined since all other variables are known.

The transducer employed was a RDP Electrosense, type E308. To use this transducer, a small device was constructed which permitted the squeezing of the load cell with the scissors as shown in Figure 3.10. Once k is determined, Equation 3.3 can be rearranged and used to determine the force the blades exerts to cut a tissue at the contact point C from the measured force data, F_M, since $\overline{OF}$ and $\overline{OC}$ are known. $\overline{OF}$ is a scissor characteristic and $\overline{OC}$ is determined from the opening angle.

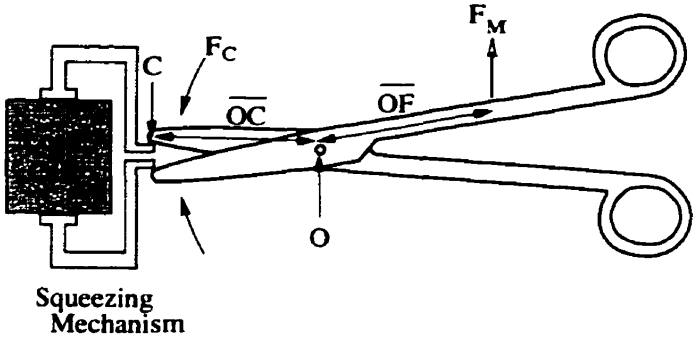

FIGURE 3.10. Set-up used to calibrate scissors.

Calibration experiments were run with a sampling frequency of 700 Hz. The closing down of the scissors on the load cell ranged from 2.4 seconds (1700 samples) to 5.6 seconds (3920 samples) per run. The k's were determined with 3 runs, each at a different $\overline{OC}$ distance, for each of the 3 scissors and an average k was obtained. In total, the number of data points for the calibration of the Mayo scissors was 10,000, for the Metzenbaum was

9,300 and for the Iris scissors was 9,700. The average constants k were found to be 0.21 V/N for the Mayo, 0.54 V/N for the Metzenbaum and 0.11 V/N for the Iris scissors.

The resulting F_C's are graphed in Figure 3.11 where the dotted lines, labelled experimental, correspond to the experimental F_C values measured with the load cell using the set up in Figure 3.10 and the solid lines, labelled calculated, correspond to the F_C's calculated from Equation 3.3 using the average k constants. The results from the fitting are good for the Mayo and Metzenbaum scissors, however the match is not as accurate for the Iris scissors.

There are several factors which can account for the errors in Figures 3.11*a* and *b*: (1) although care was taken to make the beams of the squeezing mechanism rigid, they still bent slightly, which resulted in a slight change in the angle θ and hence, a change in the $\overline{OC}$ distance which was not accounted for, (2) during experimentation, there was minor slipping of the blade, thereby again varying the $\overline{OC}$ distance which was not accounted for when solving Equation 3.4 and (3) the tests were performed dynamically by applying the force manually and hence, with uneven pressure. These factors do not explain the large errors in Figure 3.11*c* for the Iris scissors, however.

The variability of the Iris scissors can be largely explained by the fact that a quarter-bridge configuration was used, since only a quarter of the bridge was active. This configuration was used due to space limitations for the small Iris scissors, and it was felt that modifying the scissor arm to accommodate the sensor would have significantly altered the scissor dynamics. As well, a quarter-bridge had given acceptable results with the larger, less sensitive foil gauges in a previous design. It was found that, although a quarter-bridge can be used with the larger foil gauges with the 2100 Signal Conditioner by MicroMeasurements, it is not feasible in all configurations.

3.1. Statistical Analysis for k constants. Statistical error calculations were performed to give an objective measure of the goodness of fit for the average k's found. The software statistics program EcStatics for Windows was used to perform a linear regression to determine the importance of the independent variables on the dependent variable. The experimental $F_{M,cal}$ was regressed on the calculated $F_{M,exp}$ which gives an equation of the form

$$F_{M,cal} = b_1 F_{M,exp} + b_2. \tag{3.5}$$

An ideal fit would give a $b_1 = 1$ in Equation 3.5 and $b_2 = 0$. The number of data points used in the regression is 10,000 for the Mayo, 9,300 for the Metz and 9,800 for the Iris. From Table 3.1, one can see that the b_1's are close to 1 for all three scissors and the

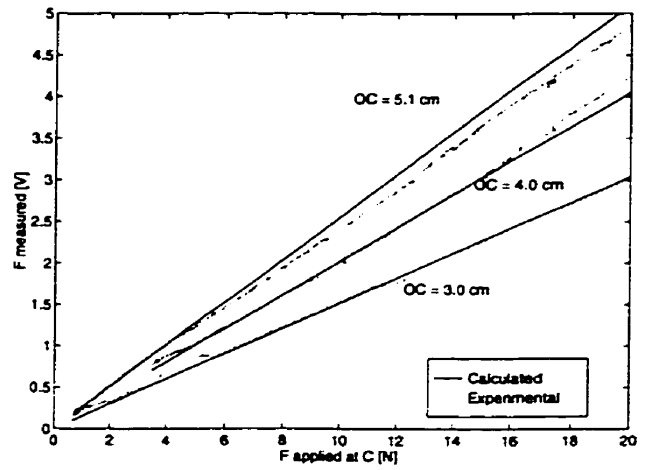

(a)

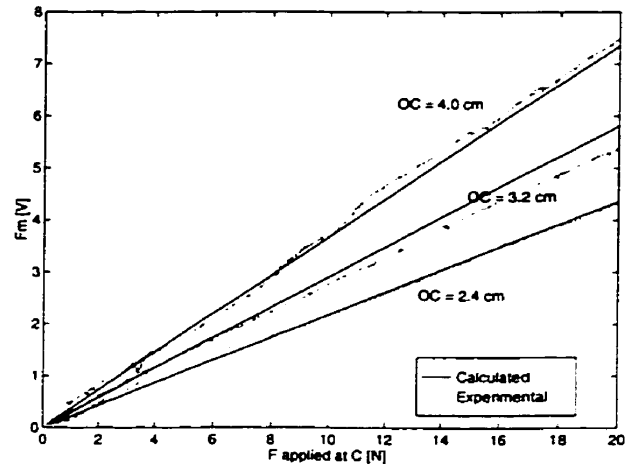

(b)

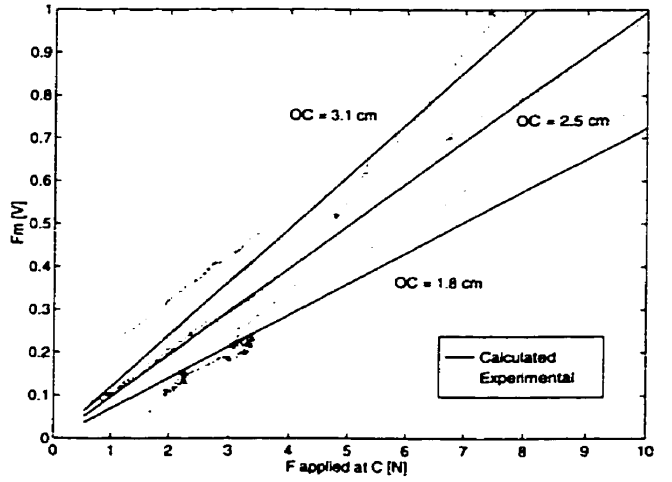

(c)

FIGURE 3.11. Calibration of (*a*) Mayo, (*b*) Metzenbaum and (*c*) Iris scissors.

b_2's are close to zero for all three scissors, only a little higher for the Iris scissors at 0.122. It is also informative to look at the t-values obtained from the regression, see Table 3.1. The lower the absolute value of the t-value, the less significant that variable is. Whereas the coefficient of $F_{M,exp}$, b_1, has a very high t-value and hence is very significant for the Mayo and Metzenbaum scissors, it is less so for the Iris scissors. This indicates a weaker relationship between the $F_{M,exp}$ and $F_{M,cal}$ for the Iris scissors and that other factors may be affecting the constant k for these delicate scissors.

	Variable	b	Std Error	t-value
Mayo	$F_{M,exp}$	0.960	0.0006	1553
	intercept	0.081	0.0029	28
Metz	$F_{M,exp}$	0.996	0.0007	1387
	intercept	-0.010	0.0038	3
Iris	$F_{M,exp}$	0.957	0.0028	337
	intercept	0.122	0.0056	22

TABLE 3.1. Summary for the regression of $F_{M,cal}$ on $F_{M,exp}$.

Another parameter which indicates the strength of the linear relationship between two variables is the simple linear correlation r which is calculated as

$$r = \frac{SS_{xy}}{\sqrt{SS_{xx}SS_{yy}}} \tag{3.6}$$

where $SS_{xy} = \sum(x-\bar{x})(y-\bar{y})$ and $SS_{xx} = \sum(x-\bar{x})^2$ and SS stands for sum of squares [21]. If $r = 1$, a perfect positive linear correlation exists between x and y. In this case, where $x = F_{M,exp}$ and $y = F_{M,cal}$, the r was calculated to be 1.00 for the Mayo, 1.00 for the Metzenbaum and 0.96 for the Iris, again indicating a better fit for the Mayo and Metzenbaum scissors.

Since the output force range is different for the three scissors, a measure was sought which would indicate the goodness of fit as a function of the range of the error compared to the range of the output. Therefore, a root-mean-square (RMS) error analysis was performed. The RMS was calculated using the equation

$$RMS = \sqrt{\sum_{n=1}^{N}(F_{M,exp}(n) - F_{M,cal}(n))^2} \tag{3.7}$$

where N is the number of data points. The results from these tests are presented in Table 3.2. The standard deviation of the error is denoted σ, the range of the values of $F_{M,exp}$ is labelled *range*, and the maximum deviation, or error, is labelled maxD. The percent error

for the RMS, E(RMS), was taken as

$$\mathrm{E}(RMS) = 100 * \left(1 - \frac{range - RMS}{range}\right) \tag{3.8}$$

and the percent error for the maxD was taken as

$$\mathrm{E}(max\mathrm{D}) = 100 * \left(1 - \frac{range - max\mathrm{D}}{range}\right). \tag{3.9}$$

	Mayo	Metzenbaum	Iris
N	10000	9300	9800
RMS	0.11	0.15	0.21
maxD	0.57	0.65	0.61
σ	0.09	0.13	0.17
$range$ [V]	7.58	9.95	2.45
E(RMS)	1.5%	1.5%	8.6%
E(maxD)	7.6%	6.4%	25.0%

TABLE 3.2. Comparison of Errors for the calculated force $F_{M,cal}$ versus experimental results, $F_{M,exp}$.

As expected, the best results were obtained for the Mayo and Metzenbaum scissors where the maximum error between actual data points and the model was 7.6% for the Mayo and 6.4% for the Metzenbaum and the average percent error was only 1.5% for both. The Iris scissors were harder to model with an average error for the F_M of 8.6% and a maximum error of 25.0%.

With the constant k's determined, the force measurements in volts can easily be converted to Newtons. These k's were used to convert the measured forces for all experiments to the force that the blade applies on the tissue at C.

4. Data Segmentation

As in speech recognition, one of the major problems encountered was the segmentation of the data. Whereas in speech recognition words run into one another, in this case, different cutting phases ran into each other. There are four distinct phases in cutting: (1) opening the scissor, (2) waiting, (3) closing the scissor, and (4) resting before opening again, see Figure 3.12. To facilitate the segmentation of the data, the velocity of the angle vector was calculated to determine where the scissor changes cutting direction. At the point of direction change, a zero-crossing in the velocity vector occurs. The zeros are few and thus make it easy to determine the beginnings and ends of different cutting phases.

In order to determine the velocity, an adaptive velocity estimation algorithm was used which provided the velocity vector in real-time [15]. The two major parts of the velocity

estimation algorithm are, one, the filtering to reduce the effects of noise and two, a least-squares approximation of the slope of the line, in an adaptive window, to obtain a velocity estimate of the angle θ.

Matlab was used to segment the data into the above mentioned sections by (1) finding all the points in the velocity vector less than some ϵ, where typically $\epsilon < 0.05$, and then (2) going through this vector to determine the zeros which are more than γ data points apart, where typically $\gamma > 100$. This gave the zero-crossings from direction changes, rather than the zeros obtained from constant position. The velocity, force and angle data of a typical run can be seen in Figure 3.12.

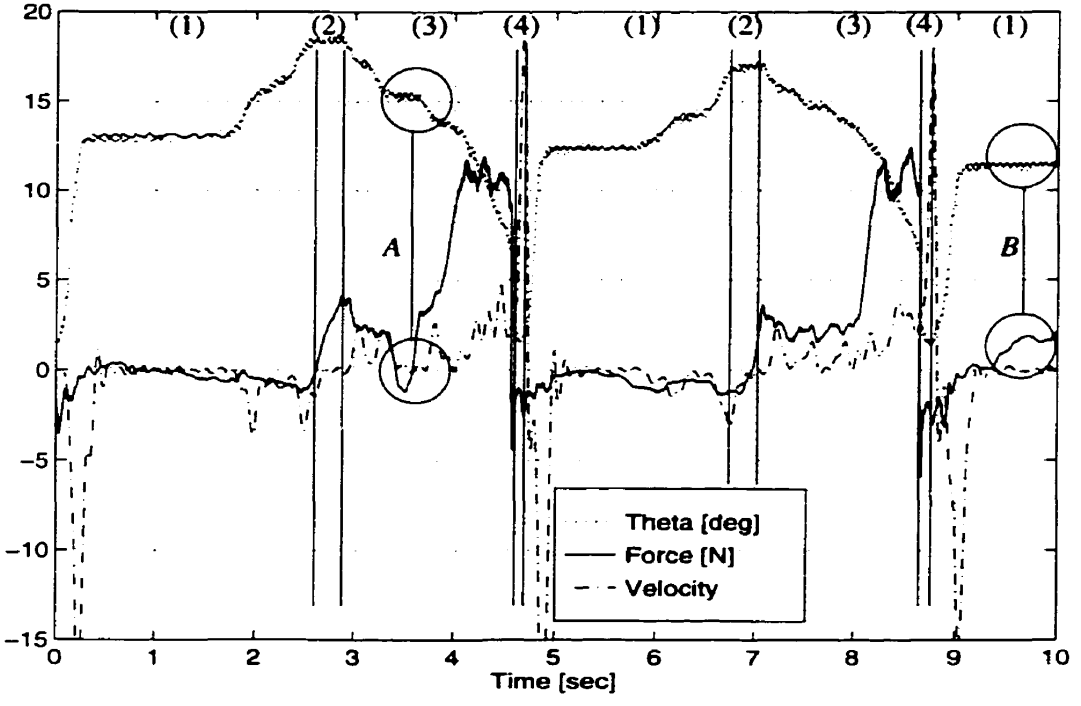

FIGURE 3.12. Force, velocity and position θ data for a typical cut with the Metzenbaum dissecting scissors. Phase (1): Opening; Phase (2): Waiting before closing; Phase (3): Closing; Phase (4): Resting before opening. Point A: pause in the closing; Point B: apply closing force while scissor at rest.

Another graph which is useful in analysing this system is that of the position θ versus the force applied, Figure 3.13. The forces which are below zero correspond to opening the scissor.

Looking at these two graphs together, one can better analyse the system. There are two complete cycles represented in Figure 3.12 with an extra Phase (1) at the end. Starting

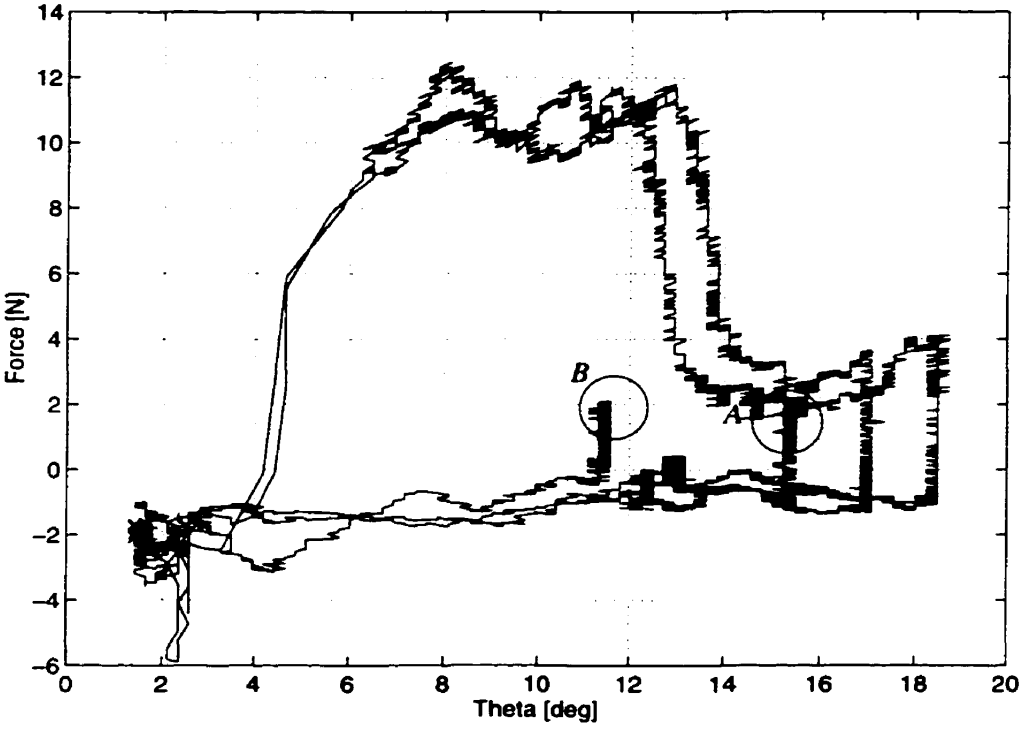

FIGURE 3.13. Force versus theta position data for a typical cut with the Metzenbaum dissecting scissors. Point A: pause in the closing; Point B: apply closing force while scissor at rest.

at time zero in Figure 3.12, there is Phase (1), opening the scissor, which is a rapid increase in the angle θ to around 13^o. The zero point corresponds to a point in the lower left-hand corner of Figure 3.13. This is then followed by a wait from 0.4 *sec* until 1.7 *sec*, where the angle remains at the 13^o, after which the scissor is again opened which then completes Phase (1) at 2.4 *sec* and 18.5^o. The complete Phase (1) is referred to as the opening curve and is the lower curve in Figure 3.13.

Phase (2), waiting before closing the scissor after it has been opened, is typically the position the doctor keeps the scissor in when not in use rather than a closed position, so to be ready to cut. However, in this run, this waiting is partially integrated into Phase (1) (the long waiting period from 0.4 *sec* to 1.7 *sec*) since there is a second opening section before the scissor is closed. From the force curve in Phase (2) from 2.4 *sec* to 2.9 *sec*, it can be seen that, although the scissor is not moving, the force increases. This is explained by a change in the scissor grip. The doctor has changed the holding grip from a pull-open grip to a push-closed grip since the position is constant but the force is increasing. Therefore, the waiting period before closing is not inactive, it is simply a methodical change in grip.

The difference between these two grips lies in where the contact is made between the finger and the inside of the scissor ring. The push-closed grip is when the fingers are contacting the inner part of the scissor rings, exerting a closing force, and the pull-open grip is when the fingers are making contact with the outer part of the scissor ring, exerting an opening force on the scissors. This change in grip causes the force reading to drift upward while the position reading remains constant at $\theta = 18.5^o$ in Figure 3.12. In Figure 3.13, Phase (2) is seen as a vertical line near 18.5^o.

At 2.9 *sec*, the scissor moves into Phase (3), the cutting phase. As the angle decreases, the force remains at around 3 N until the tissue is encountered. The closing force curve is clearly different from the opening curve. At close to 3.4 *sec* in Figure 3.12, there is a pause in the closing phase during which time the position is constant. This section is circled and labelled A in both figures. In order to stop cutting, the doctor changes from the push-grip to the pull-grip. This can be seen by the decrease in the force between times 3.4 *sec* to 3.7 *sec* during which time the position remains constant at 15.5^o. Actually, the force drifts down to the force level of the open curve (-1 N). This jump down to the opening curve can be seen as a vertical line in Figure 3.13 at 15.5^o.

Once the cutting resumes at 3.7 *sec*, the force jumps back onto the closing curve. The cutting lasts until around 4.6 *sec* when the breakthrough occurs. At the break through, the force drops off quickly to below zero as the grip changes from the closing-grip to the open-grip to restrain the scissor from closing further. The fact that the force sensors can measure the grip changes indicates their sensitivity. The complete Phase (3) is the closing curve and is seen as the upper curve in Figure 3.13.

After Phase (3), the resting period, Phase (4), is quite short and the force moves rapidly into Phase(1) again. This is witnessed by the near immediate jump to the open curve after the breakthrough. Phase (4) is typically short for this scissor type because of how the doctor uses them. With the Metzenbaum scissor, the doctor begins opening the scissor almost as soon as the breakthrough occurs. Phase (4) is more distinct for the other two scissor types.

Another complete cycle is shown in Figure 3.12 from 4.7 *sec* until 8.7 *sec*. From 8.7 *sec* until 10 *sec*, there is simply an open to roughly 11.7^o at which point the force drifts up to the closing curve level (2 N). The drift upward in the force is seen in Figure 3.13 as a vertical line near 11.5^o. This section is circled and labelled B in both figures. The doctor has changed to the push-closed grip even though the position has not changed. These grip changes will be further explored in Chapter 4 section 1.2.

5. System Identification

System identification was performed on the scissors to determine the range of frequencies which could be expected, and thus specify the minimum sampling frequency required.

To determine the bandwidth of the scissors, a disk drive motor was used to excite the scissors at different frequencies by rigidly attaching it to the scissor arm equipped with the force sensor. The response of the scissors from this excitation was measured with the strain gauges. SigLab^{TM} was employed to make Bode diagrams of the data and the Virtual Swept-Sine (VSS) operator in SigLab^{TM} was used to drive the disk drive at different frequencies in incremental steps. The set-up used can be seen in Figure 3.14. The disk drive was run

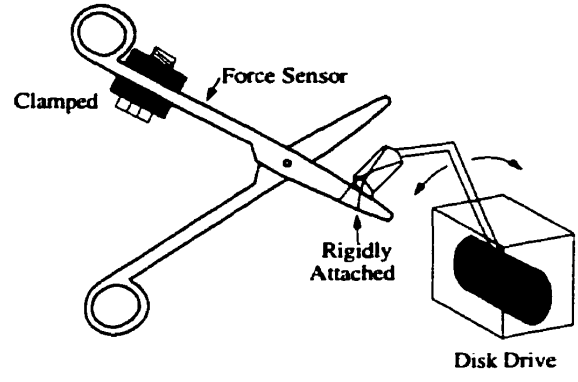

FIGURE 3.14. Set-up used to create Bode diagrams for system identification.

with a current amplifier by supplying 0.06 V output from the VSS which resulted in 0.06 Amps being supplied to the disk drive. The same conditions were used for all three scissors.

5.1. Motor Dynamics. The first step required the determination of the bandwidth of the disk drive motor itself. For this, the force transducer described in Chapter 3 section 3 was attached to the motor and the output from the transducer was used to create a Bode diagram, Figure 3.15. The force transducer has a rated bandwidth of 500 Hz.

From these experiments, it was determined that the motor has a bandwidth greater than 140 Hz. Therefore, the motor will not introduce any dynamics to the scissor system identifications until frequencies greater than 140 Hz.

5.2. Mayo Scissors. The Mayo scissors can be modelled as a second order system, having two undamped poles, see Figure 3.16. To parameterise this system, the following equation for second-order systems was fit to the data,

$$f = \frac{k w_N^2}{s^2 + 2\zeta w_N s + w_N^2} \tag{3.10}$$

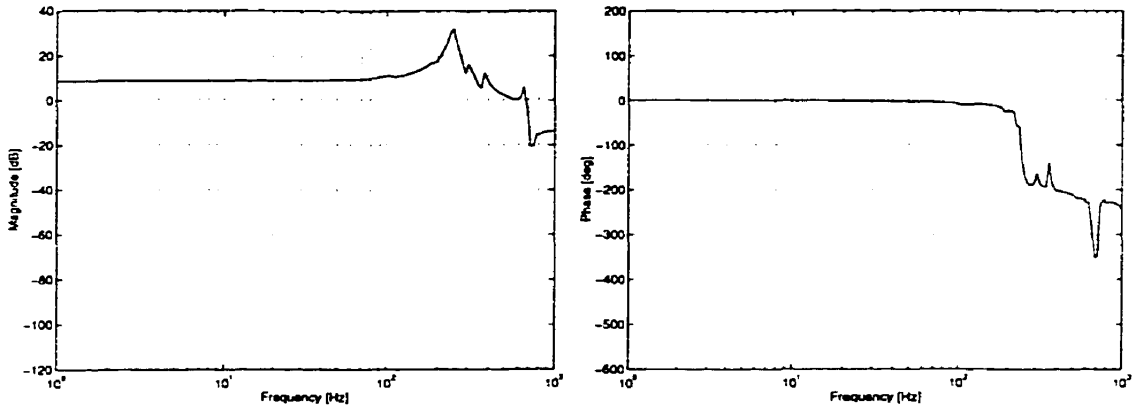

(a) (b)

FIGURE 3.15. Bode diagrams for the characteristics of the disk drive as measured using the force transducer.

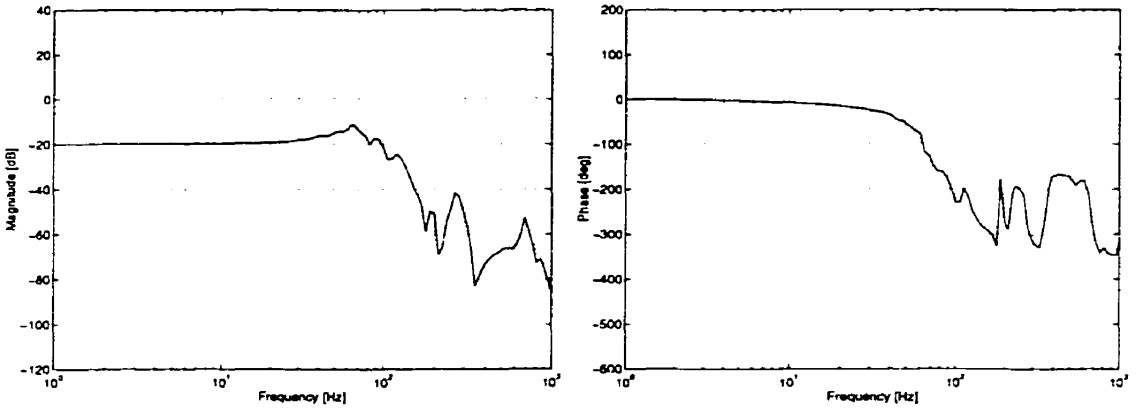

(a) (b)

FIGURE 3.16. Bode diagrams for Mayo scissors: (a) Magnitude (b) Phase.

where k is the gain, w_N is the undamped natural frequency and ζ is the damping coefficient.

From this equation, the two poles were determined to be at $s = -6.6 \pm 59.6j$. This corresponds to $w_N = 60$ Hz, $\zeta = 0.11$ and $k = 0.10$. A Bode plot of the data with the fit is presented in Figure 3.17. The Bode plot shows that the scissor passes all frequencies below 20 Hz without any distortion and actually amplifies frequencies between 20 and 65 Hz. The the cut-off frequency (-3 dB) is at 102 ± 0.5 Hz (-23.0 dB) after which all frequencies are attenuated by the scissor itself. Note that due to the fact that this Mayo scissor has been slightly altered for the mounting of the strain gauges, this transfer function may not be identical to those of other Mayo scissors.

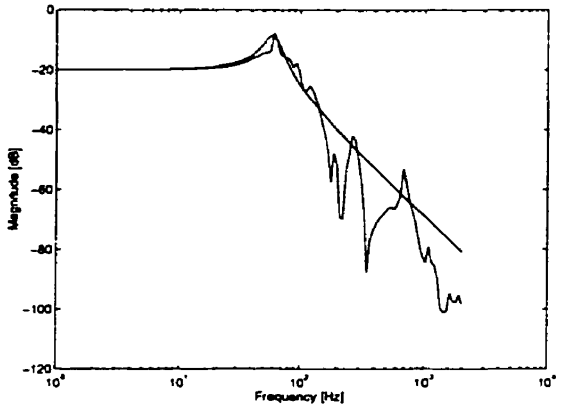

FIGURE 3.17. Bode plot fit to original data for Mayo.

5.3. Metzenbaum Scissors. A similar second order transfer function can be observed for the Metzenbaum scissors, Figure 3.18. The major difference is in the gain for the two scissors. This results is a combination of the sensor gain and the scissor mechanical gain differences. Since the Metzenbaum are much thinner than the Mayo, they give a higher response for the same excitation. A fitting in Matlab gave the poles at $s = -2.34 \pm 39.9j$

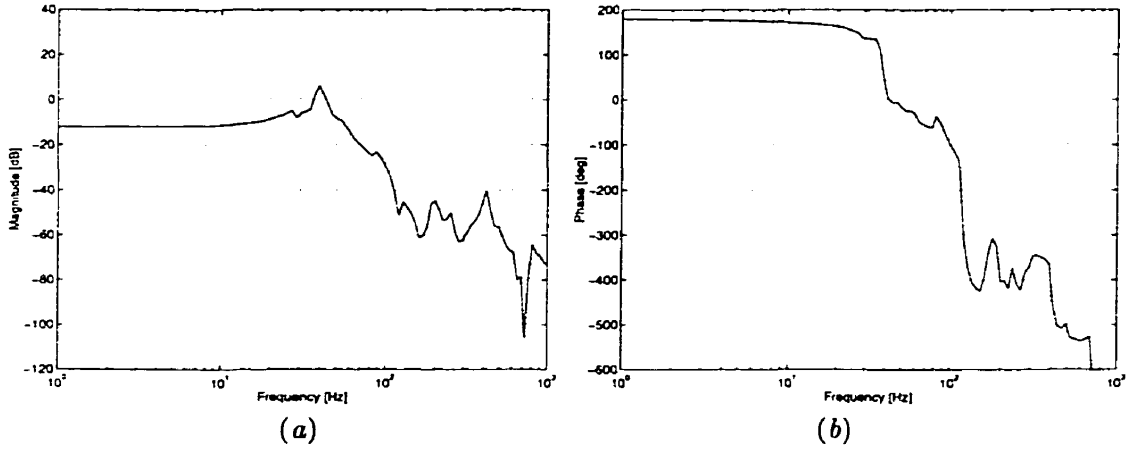

(a) (b)

FIGURE 3.18. Bode diagrams for the Metzenbaum scissors: (a) Magnitude (b) Phase.

which corresponds to $w_N = 39$ Hz, $\zeta = 0.06$ and $k = 0.25$. From the Bode plot of the fit versus the original data, Figure 3.19, the cut-off frequency (-3 dB) for the Metzenbaum was determined to occur at -15.1 dB which corresponds to 61 ± 0.5 Hz.

5.4. Iris Scissors. Similarly for the Iris scissors, the original Bode diagrams are presented in Figure 3.20. The poles were determine to be at $-12.6 \pm 68.9j$, which corresponds to $w_N = 70$ Hz, $\zeta = 0.18$ and $k = 0.19$. The fit versus the original Bode plot data is

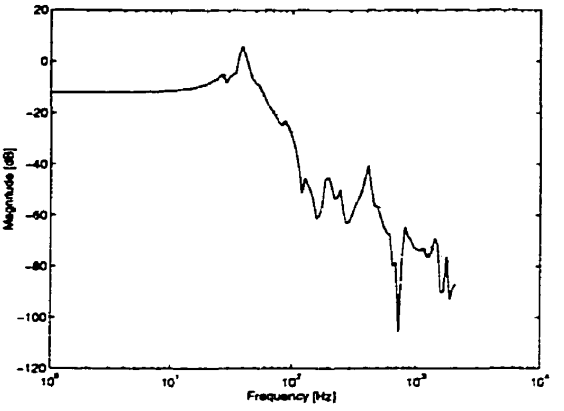

FIGURE 3.19. Bode plot fit to original data for Metzenbaum.

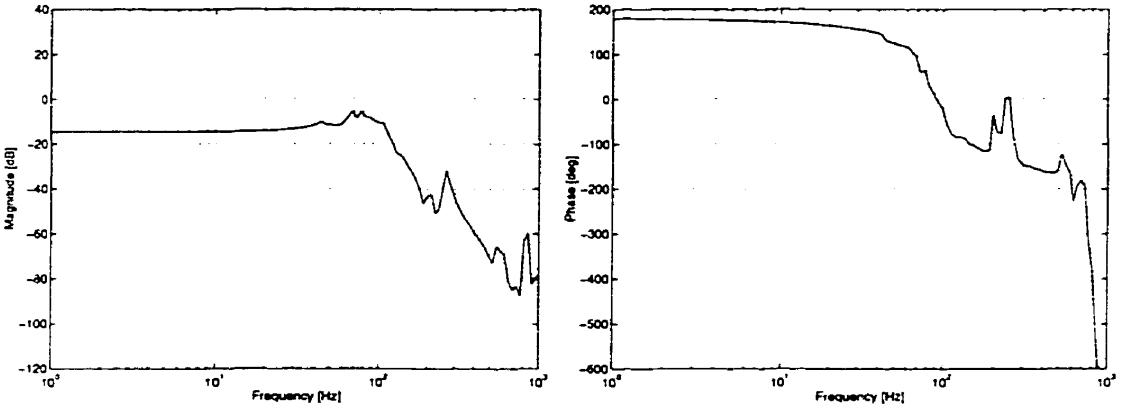

(a) (b)

FIGURE 3.20. Bode diagrams for Iris scissors: (a) magnitude (b) phase.

presented in Figure 3.21. From this figure, the cut-off frequency is 118 ± 0.5 Hz for -14.6 dB.

Since the maximum frequency which can be measured by the strain gauges for the three scissors mounted in this configuration is no greater than 118 Hz, the sampling frequency was set at approximately 10 times the maximum detectable frequency, or 1000 Hz. From these experiments, one can conclude that, for the three scissors, the maximum frequency which a force-feedback device would need to provide for the realistic force playback of virtual scissors is 100 Hz. Any signal above 100 Hz is automatically damped out by the scissors themselves and therefore, undetectable.

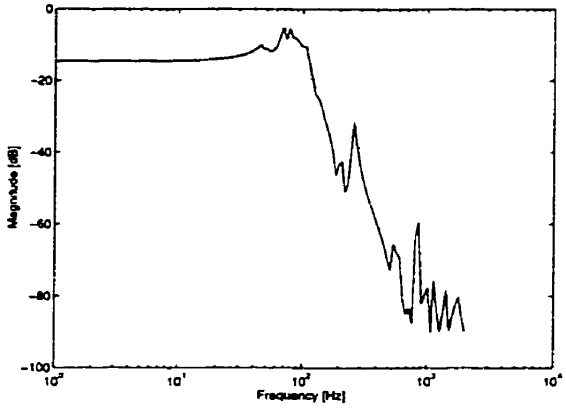

FIGURE 3.21. Bode plot fit to original data for Iris scissors.

CHAPTER 4

Data Analysis and Results

The main goals of this research were to investigate:
(1) What do the force cutting curves for difference tissue types look like and is there a measurable difference between different tissues?
(2) What frequency components are in the signal and what knowledge can these provide?
(3) Is the force measurement dependent on the velocity and if so, how?
(4) Are there any invariants between tissues or scissors which can be determined?

To answering these questions, the data acquired in Chapter 3 is analysed using statistical methods. Also instructive is the valuable knowledge obtained upon working with the doctor.

1. Tissue Differences

The tissues compared are from experiments performed upon a sheep and two rats. More specifically, the tissues are skin from the abdominal region, the abdominal muscle wall, the liver and the calcaneal (or Achilles) tendon. The abdominal muscle wall is actually composed of three layers, the oblique internal muscle, the oblique external muscle and the transversal abdominal. These layers were not separated but rather cut as one tissue. For the sheep experiments, it was possible to also test muscle-rectus fascia[1] since it was available in abundance in the fatty abdominal area of the sheep. The rats, however, had very limited fascia as they were leaner. The tissues which have an orientation were tested in the longitudinal (L) and transversal directions (T).

While these tissues would not normally be cut with scissors in a surgical situation, they have been selected for these preliminary tests due not only to their accessibility and

[1] Fascia is a connective tissue covering or binding together body structures.

relative abundance, but also because of their variability in properties. Tissues with large differences were sought in order to establish how varied they need to be for a difference to be registered by the force sensor and hence sensed by the operator. Experiments were run at two cutting speeds, slow and fast, which were judged by the doctor while cutting. Generally, slow corresponds to a speed less than 15 deg/sec and fast is greater than 15 deg/sec. Once the experimental procedure has been established, further research will be necessary to determine more accurately the properties of all the relevant tissues.

Before looking at the specific force curves in detail, the maximum of the average force applied, $\max\tilde{F}_A$, for each tissue type is presented to establish general trends, see Table 4.1. The average force applied, $\tilde{F}_A$, is actually the curve obtained by (1) stepping along in θ and (2) averaging the force applied by the blade on the tissue at the contact point C (F_A) at each θ for several runs. Also presented is the $\tilde{F}_A$ at the break-through angle, θ_B, which will be explained in more detail in section 4. The corresponding graphs can be found in Appendix D. The missing values in Table 4.1 are a result of experimental limitation and sampling errors which will be discussed later in more detail in section 1.7.2.

1.1. Maximum Average Force. Although the numbers in Table 4.1 are not exact quantitative measures for the forces required to cut these tissues due to limited sample set sizes, they do allow for qualitative comparisons between different tissues. For each tissue type, the data files were limited to 20 seconds of recording, which generally allowed for 3-5 cuts. For most tissues, two data files were collected per tissue for each of the conditions, speed, scissor type and cutting direction when applicable.

Looking first at the two upper sections of Table 4.1 for the Mayo and Metzenbaum scissors, the sheep tissues generally require more force to cut than the rat tissues. For the Mayo rat experiments, the $\max\tilde{F}_A$ is below 10.2 N for all runs except the tendon, which resulted in $\max\tilde{F}_A = 22.8$ N. However, for the sheep experiments with the Mayo scissors, the forces were higher, reaching as high as 20.5 N for the longitudinal, fast cutting of skin. Similarly for the Metzenbaum scissors, the rat tissues (excluding the tendon) were all below 8.1 N. For the sheep experiments with the Metzenbaum scissors however, the $\max\tilde{F}_A$ reached as high as 19.3 N. This trend between rat and sheep tissues could have been predicted upon visual inspection since the sheep tissues are much thicker and stronger than the corresponding rat tissues.

The tendon is the only tissue which did not change dramatically in the $\max\tilde{F}_A$ required. In order to cut the massive sheep Achilles tendon, it was necessary to split it and cut only the number of strands that could reasonably be cut by the scissors. This resulted in a

Scissor	Tissue	Rat		Sheep	
		max$\bar{F}_A$ [N]	max$\bar{F}_A$ at θ_B [N]	max$\bar{F}_A$ [N]	max$\bar{F}_A$ at θ_B [N]
Mayo	Blank (slow)	6.6	6.6	8.0	7.9
	Blank (fast)	6.4	6.2	7.3	6.5
	Skin (L, slow)	8.0	5.8	17.6	13.5
	Skin (L, fast)	8.7	6.2	20.5	9.2
	Skin (T, slow)	8.4	5.2	16.4	-
	Skin (T, fast)	7.8	5.0	16.4	9.2
	Muscle (slow)	10.2	6.8	-	-
	Muscle (L, fast)	-	-	5.8	4.6
	Muscle (T, fast)	-	-	9.1	5.0
	Liver (slow)	6.1	5.0	-	-
	Liver (fast)	5.8	4.5	8.3	4.4
	Fascia (slow)	-	-	7.8	4.6
	Fascia (fast)	-	-	8.7	5.5
	Tendon	22.8	-	24.6	-
Metz	Blank (slow)	3.1	1.6	4.0	3.7
	Blank (fast)	3.6	2.8	2.6	1.1
	Skin (L, slow)	7.0	5.9	17.5	13.5
	Skin (L, fast)	5.9	4.2	16.9	7.4
	Skin (T, slow)	-	-	13.2	-
	Skin (T, fast)	8.1	6.7	19.3	15.9
	Muscle (slow)	-	-	-	-
	Muscle (fast)	2.4	2.3	-	-
	Liver (slow)	2.5	2.2	-	-
	Liver (fast)	1.6	1.4	7.1	3.0
	Fascia (slow)	-	-	-	-
	Fascia (fast)	-	-	6.0	3.4
	Tendon	30.5	-	-	-
Iris	Blank (slow)	5.1	1.0	4.7	-
	Blank (fast)	3.0	1.1	7.2	1.3
	Skin (L, slow)	22.6	9.4	44.8	-
	Skin (L, fast)	23.4	14.1	32.6	15.7
	Skin (T, slow)	17.3	11.1	-	-
	Skin (T, fast)	18.2	11.3	-	-
	Muscle (slow)	16.6	8.3	-	-
	Muscle (L, fast)	-	-	14.0	6.7
	Muscle (T, fast)	22.8	3.6	27.0	9.6
	Liver (slow)	10.2	-	-	-
	Liver (fast)	10.7	4.9	21.2	10.4
	Fascia (slow)	-	-	12.5 [2]	7.5
	Fascia (fast)	-	-	17.7	12.8
	Tendon	-	-	-	-

TABLE 4.1. The maximum of the average applied force F_A for different tissue types and the average applied force F_A at the break-through angle, θ_B (θ_B=6.5° for Mayo, 7.2° for Metz and 5.2° for Iris).[L=longitudinal, T=transversal]

bundle close to the size of the rat Achilles tendon, which explains why the measured forces are approximately equal.

1.2. Comparing blanks and liver. The experiments labelled blank actually indicate the $\max\tilde{F}_A$ for the opening and closing of the scissors in thin air. One might expect these runs to have the lowest $\max\tilde{F}_A$. Although this is true for the Iris scissors, it is not true for the Mayo and Metzenbaum scissors where the liver cut requires actually less force than the blank. For example, the average $\max\tilde{F}_A$ for the Mayo blank was close to 7.0 N, whereas for the rat liver it was only 5.8-6.1 N. Similarly for the Metzenbaum, the blank had a $\max\tilde{F}_A$ of approximately 3.3 N, but for the rat liver it only registered 1.6-2.5 N. However, for the Iris scissors, the rat liver required much more force to cut, approximately 10.2-10.7 N versus 5 N for the blank. The results for the Iris scissors will first be explored in section 1.2.1, after which the question of the Mayo and Metzenbaum will be addressed in section 1.2.2.

1.2.1. F_A *of the Iris scissors.* Looking at the Iris scissors, an interesting observation can be made. All tissue cuts performed with the Iris scissors require more force when compared to the results from the Mayo and Metzenbaum scissors. Whereas the shorter arm length has no bearing on the measurement of F_A, the shorter blade length does. The Iris blade length ranges from 0.5 to 0.75 the length of the Metzenbaum blade length, as a function of the scissor angle. Therefore, the force to cut should be from 2 to 1.5 times higher. However, the forces are typically 2 to 3 times higher than the Metzenbaum scissors, therefore other factors must exist to account for these differences.

Effectively, the Mayo and Metzenbaum scissor blades are equipped with tungsten carbide inserts which makes their blade edges sharper and stronger than the Iris blades. As well, since the blades themselves are thicker for the Mayo and Metzenbaum scissors, they are less likely to be pushed apart by the tissue. Therefore, the Mayo and Metzenbaum blades actually shear the tissue in front of the cutting point due to their sharper blades. The small Iris scissors are not able to shear the tissue in this manner and therefore require more force to cut the tissues. The shearing which is occurring actually results in a decrease in F_A since not all of the cutting is occurring at the contact point of the two blades. Therefore, it is clear why the liver is higher for the Iris scissors than the blank since for the Iris, even a thin tissue is hard to cut. This does not resolve the question of why the F_A for the liver experiments for the Mayo and Metzenbaum scissors are lower than their respective blank cuts however.

1.2.2. F_A *of the Mayo and Metzenbaum scissors.* To explain why the Mayo and Metzenbaum liver runs register a lower force than the blanks, it was hypothesised that

the blood of the liver tissues were lubricating the scissors since the liver is the most moist of the tissues tested. However, this effect was not reproducible in laboratory experiments where, a batch of experiments were performed under dry conditions, after which another batch was run with WD40, car oil, sprayed on the scissors. The results from these two experiments gave virtually the same F_A versus θ curves for each of the three scissors. Upon closer inspection of these curves, however, it was noticed that the blank runs performed by the student were lower than the blank runs performed by the doctor. In Figure 4.1, the blank runs for the student and doctor are shown side-by-side for each of the three scissors.

Whereas the doctor registers a max$\bar{F_A}$ of 8 N to close the Mayo scissors from Table 4.1 (which is shown graphically in Figure 4.1*a*), the student registers nearly half of that, 4.1 N from Figure 4.1*b*. Similarly for the Metzenbaum scissors, the doctor registers up to 4 N and the student registers a maximum of 2.9 N, see Figures 4.1*c* and *d*. For the Iris scissors, the doctor resulted in a max$\bar{F_A}$ of 7.2 N and the student a maximum of 4.7 N, see Figures 4.1*d* and *f*. Therefore, the grip, as well as the tissue and scissor types, affect the force experienced. The grip used is probably a strong function of training and reveals that it is important to involve trained surgeons at these early stages of research.

1.3. Grip Change Effects. Evidence that the grip affects the F_A value can also be witnessed in another feature of the graphs, which is an increase or a decrease in the force even when the scissor angle θ is not changing, as was previously introduced in Chapter 3 section 4. This effect can be seen first in Figure 4.2 at around 11^o on the opening curve, where there is a momentary change in the cutting direction. This is seen as a rapid increase in F_A at 11^o, which is a results of a brief closing of θ to 10^o (circled in figure). After this brief closing (decrease in θ and increase in F_A) the F_A again goes down to the force level of the rest of the open curve as the scissor is completely opened. Clearly, the short change in direction results in a momentary jump up to the blank closing curve, as it is depicted in Figure 4.1*d* for the student Metzenbaum blank run since the paper cuts were performed by the student. Looking at Figure 4.2, it is important to keep in mind that there are many runs overlapped.

It is not necessary for the θ to change at all, however, in order for the force to jump up onto the closing curve. These rapid rises in F_A in the opening curve are also visible in data where there is no actual closing of the scissor, but only a pause in the opening, as in Figure 4.3 at 11^o (circled in figure).

Clearly, in order to have the blades change direction, the grip must change from an opening grip to a closing grip. However, it appears that there is also a grip change involved to stop opening the scissor since there is a rapid increase in F_A even when there is no closing

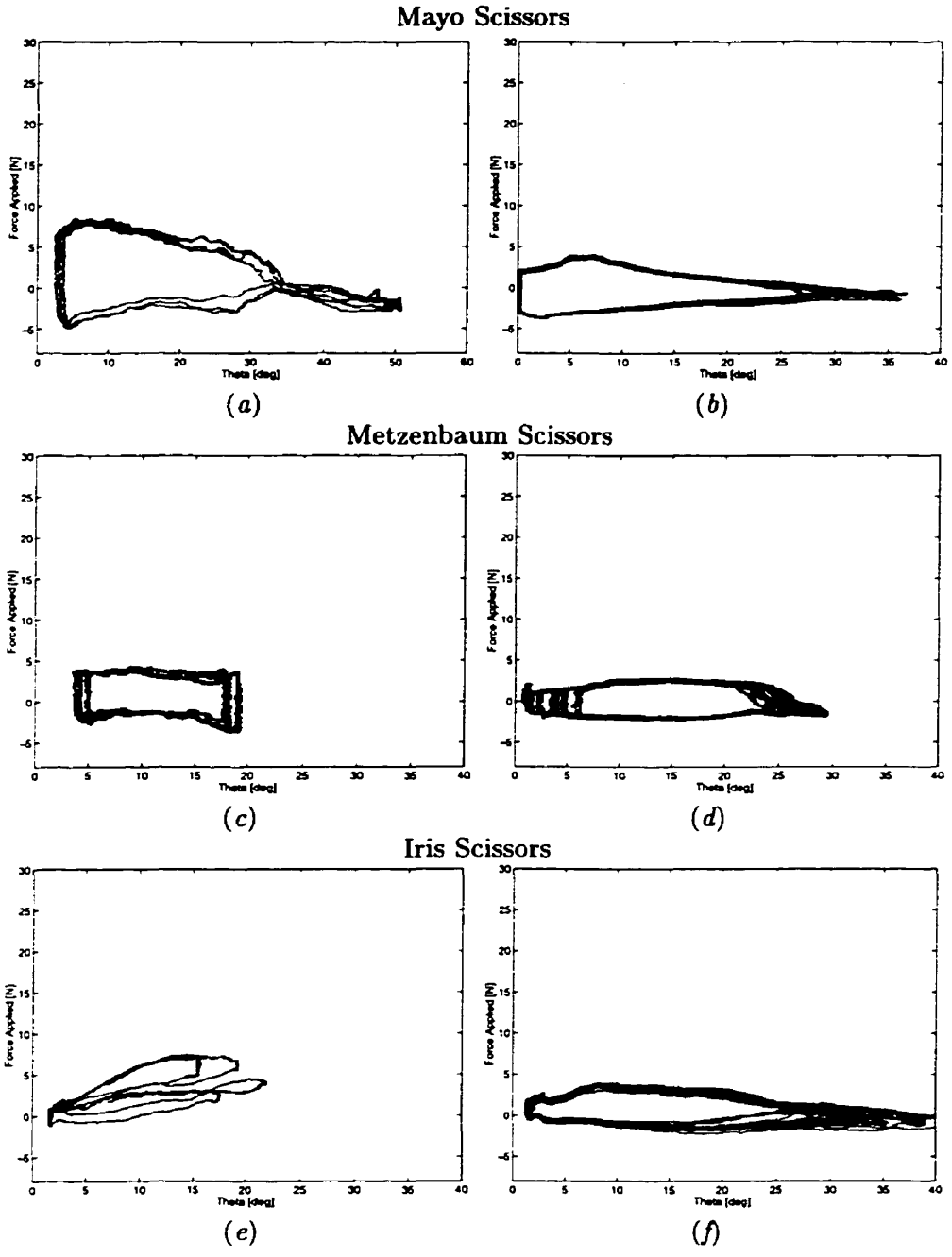

FIGURE 4.1. Comparison of blank runs for Mayo scissors between (*a*) doctor and (*b*) student; Metzenbaum scissors for (*c*) doctor and (*d*) student; and Iris scissors (*e*) doctor and (*f*) student.

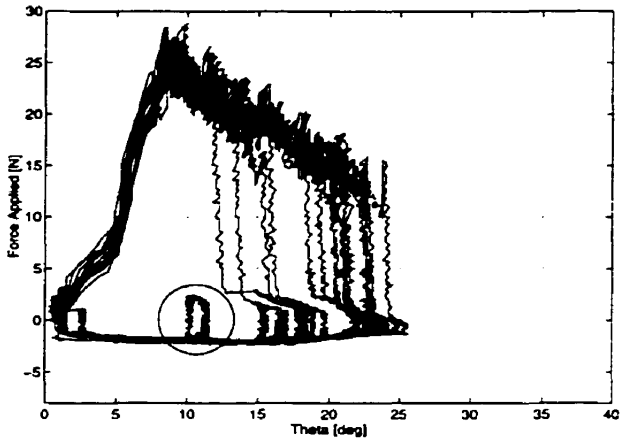

FIGURE 4.2. Effect of grip change on the measured F_A. Data taken with Metzenbaum scissors cutting four sheets of paper.

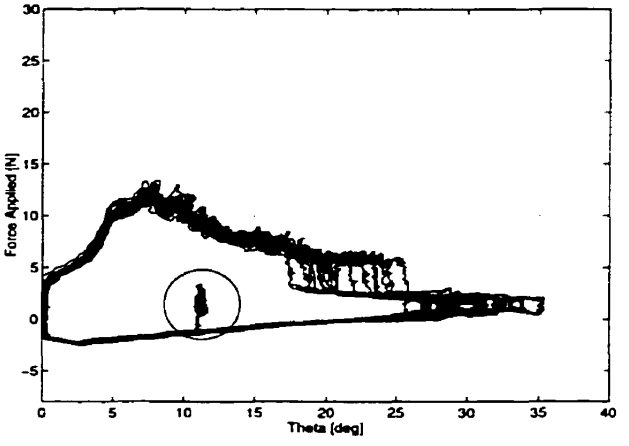

FIGURE 4.3. Effect of grip change on the measured F_A where the angle does not vary during the grip change. Data taken with Mayo scissors cutting two sheets of paper.

action. This again implies that the grip has a strong influence on the forces read. As a note, it is also the grip change that causes the abrupt increase in F_A once the scissor has been completely opened, typically near 30^o.

With this grip effect in mind, another explanation which may account for the low force readings for the liver experiments for the Mayo and Metzenbaum experiments maybe that the doctor changes his grip from a power grip to a more delicate grip, already anticipating the lower resistance of these soft materials. That is, even though the doctor may try to keep the grip constant, it is like opening a door which habitually sticks. The day someone lubricates it, everyone passing through the door slams the door open, expecting it to resist.

1.3.1. *Determining Grasp.* To further investigate this grip effect, Cutkosky's grasp taxonomy for the design of robotic hands for manufacturing tasks was investigated (see Appendix E) [4]. The taxonomy classifies the manipulation of objects depending on the object geometry and the task power requirements. In the taxonomy, the first distinction between grasps is a power grasp versus a precision grasp. Whereas the power grasp is used when there is an emphasis on security and stability, the precision grasp is used when dexterity and sensitivity are important. Applying this knowledge here may indicate that the doctor uses a different power grasp depending on the resistance of the material to cut.

As well as task, personal preference will determine how a doctor will hold the instruments. A typical grasp for surgical scissors is presented in Figure 4.4*a* (see Appendix F for figures on how other surgical instruments are held). In this figure, the thumb is inserted in one ring of the handle and the ring finger in the other. This could also have been the middle finger or little finger, depending on the doctor and the scissor type. It is recommended to

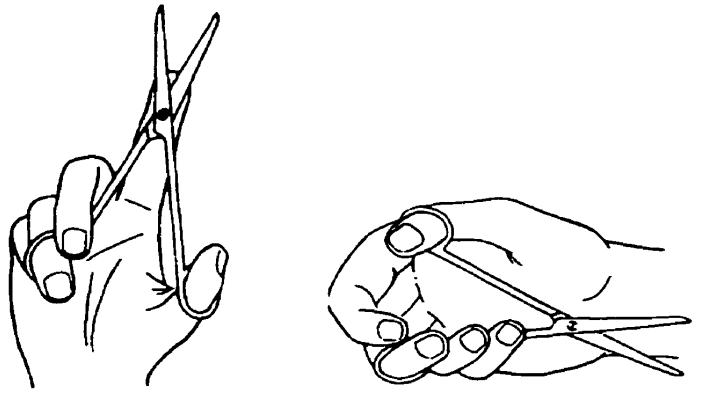

(*a*) (*b*)

FIGURE 4.4. Different ways to hold surgical scissors (picture taken from [19]).

place the index finger on the joint of the scissor to steady it. Naturally, if the scissor arm is too long, this is not possible. Equally, for an ambidextrous person, a grasp such as the one in Figure 4.4*b* can be used to cut from left to right while holding the scissors in the right hand.

1.4. Variability in Iris scissors. This grip effect may explain the high variability experienced with the Iris scissors which was mentioned earlier in Chapter 3 section 3. This variability can be seen in Figure 4.1*e*, where there are four cuts performed by the doctor overlapped. This high degree of variability is not seen in the student runs, however, as shown in Figure 4.1*f*, where there are over ten cuts overlapped. One reason the doctor may have such a large variability in scissor measurements may be related to hand size. Since the

Iris scissors are comparatively small, the doctor's larger and stronger hands may actually be bending the scissor arms differently than the student.

As well, another side-effect of the quarter-bridge configuration is probably appearing. Since this gauge configuration is more sensitive, the student was careful not to touch the strain gauge while cutting, whereas the doctor used a more natural grip so as not to alter the scissor dynamics. The possible intermittent, direct touching of the strain gauges could also contribute to the large fluctuations as a result of temperature and pressure effects. For these reasons, the results obtained from the Iris scissors may not be reliable and are included only for completeness.

1.5. Contact between Object and Scissor. Another observation which can be made from Figures 4.2 and 4.3 is that, it does not seem to matter what the incident angle is (where the scissor makes contact with the object), the F_A immediately jumps to the same closing curve. That is to say, looking at Figure 4.2, the curve which is the most inside starts closing at around 15^o where the F_A is approximately -2 N. When the scissor starts closing, the blade has made no contact with the object and therefore, the F_A is close to 3N, which corresponds to being on the blank closing curve for this scissor. Then, near 12^o, there is contact with the object being cut and the F_A rises almost instantly to 20 N to meet the same closing curve created by runs where the contact was made much sooner, i.e. at 20^o. Although this result is hard to predict for these experiments since the 3-space position is not monitored, it is easy to model once the relative scissor and object positions are known.

1.6. Longitudinal versus Transversal. Returning to Table 4.1 and looking at the curves for cutting skin in Appendix D, one can see that within each scissor category, the skin experiment results were not exactly the same. As well, there does not seem to be a direct relationship between the cutting direction and the amount of force required. For example, for the Mayo scissors, the slow longitudinal cutting of skin has a lower $\max\bar{F_A}$ then the slow transversal direction, but a higher $\max\bar{F_A}$ than the fast transversal direction. A statistical analysis was therefore performed to determine if there was a significant difference between the forces required to cut tissues in the two cutting directions, longitudinal and transversal. As no accurate model exists yet, a sum squares of error (SEE) analysis was used to compare the force curves. A significant difference between curves was taken as a difference in the SSE between the two directions, $SSE_{L,T}$, which is greater than the variability between the runs in any one direction, SSE_L and SSE_T. The SSE calculated for the variability in the

transversal direction is calculated as

$$\mathrm{SSE}_T = \sum_{i=1}^{\mathrm{N_T}} (\mathrm{F}_{T,ave} - \mathrm{F}_{T,i})^2 \tag{4.1}$$

where $\mathrm{F}_{T,ave}$ is the average force for the transversal cuts, $\mathrm{F}_{T,i}$ is the force of the transversal cut for run i and $\mathrm{N_T}$ is the total number of runs in the transversal direction. In the longitudinal direction, this is expressed as

$$\mathrm{SSE}_L = \sum_{i=1}^{\mathrm{N_L}} (\mathrm{F}_{L,ave} - \mathrm{F}_{L,i})^2 \tag{4.2}$$

where $\mathrm{F}_{L,ave}$ is the average force for the longitudinal cuts, $\mathrm{F}_{L,i}$ is the force of the longitudinal cut for run i and $\mathrm{N_L}$ is the total number of runs in the longitudinal direction. The sum square of the error between the two average curves was calculated as

$$\mathrm{SSE}_{T,L} = \sum (\mathrm{F}_{L,ave} - \mathrm{F}_{T,ave})^2. \tag{4.3}$$

So, if $\mathrm{SSE}_{T,L}$ is greater than both SSE_T and SSE_L, then the two directions were taken as significantly different. The results from this analysis are shown in Table 4.2.

Scissor	Tissue	max(SSE_T, SSE_L)	$\mathrm{SSE}_{T,L}$	Statistically different?
Mayo	Skin (sheep, slow)	3.1	1.5	N
	Skin (sheep, fast)	6.1	1.4	N
	Skin (rat,slow)	1.3	0.9	N
	Skin (rat,fast)	2.3	1.1	N
	Muscle (sheep)	0.6	2.4	Y
Metz	Skin (sheep, slow)	4.4	2.9	N
	Skin (sheep, fast)	6.1	1.4	N
	Skin (rat, fast)	3.5	2.2	N
Iris	Skin (rat, slow)	3.4	8.6	Y
	Skin (rat, fast)	4.6	4.1	N
	Muscle (sheep)	4.5	10.9	Y

TABLE 4.2. Comparing transversal and longitudinal directions for cuts.

1.6.1. *Cutting Direction Results for Skin.* For the Mayo and Metzenbaum scissors, the differences between transversal and longitudinal cuts for both the rat and sheep skin were not significantly different (for both cutting speeds). However, for the Iris scissors, the rat skin cut slowly registered as significantly different for the transversal and longitudinal directions from Table 4.2. It is not certain, however, if this is a by-product of the known variability of these scissors or if indeed, these small scissors are sensitive to the differences

in the longitudinal and transversal directions of skin. Unfortunately the fast skin cuts do not verify this result, but that could equally be a result of the variability.

The longitudinal direction for skin was taken as the one which runs along the axis of the body, hence the transversal is the one which runs perpendicular to the axis of the body. Looking back at the results from Table 4.1, the max$\bar{F}_A$ for the longitudinal direction is approximately 23 N for the Iris scissors, whereas it is approximately 17.8 N for the transversal skin direction. Since skin fibers are aligned with the horizontal axis of the body, the longitudinal force should be higher. As this is the result found, the more delicate Iris scissors may indeed be sensitive to the cutting directions. However, more experimentation is required to verify this result.

1.6.2. *Cutting Direction Results for Muscle.* The two cutting directions were significantly different for the muscle cuts with both the Mayo and Iris scissors where the $SSE_{T,L}$ is greater than the maximum between SSE_T and SSE_L. Muscle fibers are highly oriented strands which accounts for this result.

The Young's modulus (E) for dog muscle (*in-vivo*) along the fibers is 0.50 ± 14% MPa and across the fibers is 0.79 ± 24% MPa [6]. This gives a difference of 0.29 MPa between the two cutting directions. If E could be found for sheep and rat muscle, perhaps it could serve as a guideline for the difference in Young's modulus (i.e. greater than 0.29 MPa) which is required before there is haptic resolution of tissues. This would require further experimentation with other tissues for which the Young's modulus is known.

A further observation is possible with the Young's modulus by looking at the ratio between the Young's moduli for the longitudinal and transversal directions for the dog (0.5/0.79 = 0.63). Comparing this ratio to the ratio of the longitudinal to transversal forces measured for the muscle cuts with the Mayo scissors from Table 4.1, the same 0.63 (5.8 N/9.1 N) is obtained. Similarly for the Iris scissors, the ratio of the cutting forces for the longitudinal to transversal muscle cuts works out to 0.52 (14.0 N/27.0 N), which is within the error margins for the Young's moduli given above. This provides further evidence that investigation into the Young's modulus is merited as a means to use the known static data to provide information about the dynamic system.

From this analysis, the Mayo and Metzenbaum scissors seem to be insensitive to the small changes in force required to cut in longitudinal and transversal skin directions. Therefore, for the simulation of skin with these scissors, it seems reasonable that the same model could be used for both cutting directions. However, since the muscle has a much larger difference in force required to cut between directions, due to the high degree of orientation in the muscle fibers, a simulation would require two muscle models, one for each direction, to reproduce this effect.

1.7. Tissue variabilities. One observation made during the acquisition of the experimental data in a surgical environments was the variance between tissue samples. This is clearly a problem since experiments performed in controlled laboratory settings were much more consistent.

1.7.1. *Tissue Strength.* In part, the differences between tissues of the same type are due to the fact that the strength of the layers change from region to region in the animal. That is, the skin near the outside of the stomach area is thicker and tougher than the skin closer to the centre. During experimentation, care was taken to use tissue from only a small region. However, there were many different cutting conditions run which required a large quantity of uniform tissue.

To understand the effect that the thickness and strength of the tissue layer has on the force, one must examine how the tissue is being cut. As described in section 1.2 of this chapter, the force applied is a result of the cutting which is occurring at the contact point and the interaction of the tissue ahead of the cutting point. This includes the squeezing and shearing of the tissue which lies ahead of the blades. As the angle θ gets smaller, the amount of tissue squeezed between the blades increases since most tissues tested were relatively thin (less than 3 mm). Therefore, the force applied increases as the scissor closes instead of remaining constant. In other words, instead of a tissue applying a constant force along the blade as an innate property of the tissue strength, there is also the contribution of the squeezing that the blades are exerting ahead of the contact point, which results in a gradual increase in the F_A as the scissor closes, as can be seen in Figure 4.2.

1.7.2. *Tissue Preparation.* For each run, a piece of tissue needed to be prepared and isolated from the surrounding layers. This involved scraping away excess fascia to keep the tissue thickness relatively constant and pulling the tissue out so that it was accessible. The doctor took care to remove as much of the surrounding tissue, however there is an inherent trade-off between tissue preparation and time, and hence, post-mortem effects. Therefore, the thickness varies as an innate property of the tissue and as a function of the amount of other tissues sticking to the tissue of interest. Hence, it is only feasible to get an approximately even sample from run to run.

This is not a problem if the sample sizes are very large, but that is not the case here. This brings up another issue which is mentioned by Duck [6]. These experiments are performed on one sheep and two rats, which does not allow for an average between animal ages or sizes. Although the exact thickness is less important in this work where general trends are sought, it is an important factor to keep in mind for future experiments.

Another problem encountered was the folding over of the prepared tissues due to the tissue surface tension. The tissues, as mentioned, had to be exposed, so they were held

up with forceps clamped down near the corners of the tissue to hold it taut. Initially, the assisting surgeon was holding the tissues just below the corners and therefore, the skin had no support in the middle. This resulted in the edge folding over on itself, resulting in a much larger F_A since the tissues were twice as thick. This effect can be seen in Figure 4.5 where two runs were performed under the same conditions, longitudinal and fast, but give very different results. The F_A measured when the skin was folded over was nearly twice as much,

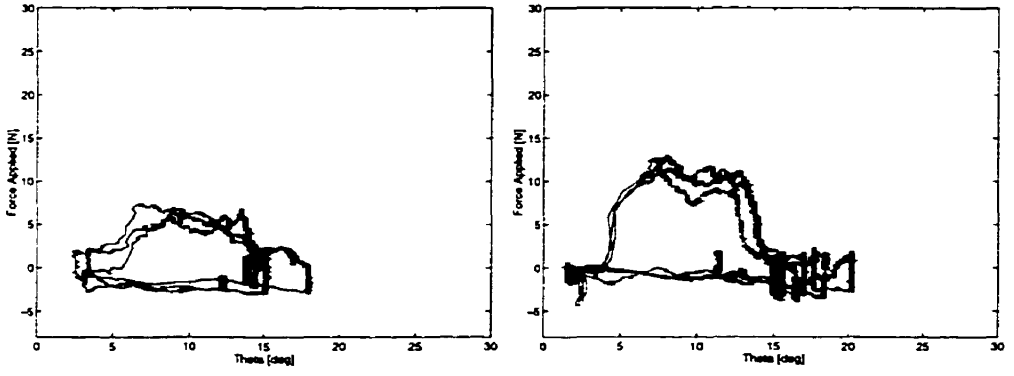

FIGURE 4.5. The effect of having the tissue layer folded over. Both curves are for the fast, longitudinal cutting of rat skin with the Metzenbaum scissors where in (*a*) the skin is normal and in (*b*) the skin is folded.

approximately 12 N versus 6 N. Unfortunately, this problem was not identified until part way through experimentation. Although most of the tests were repeated, similar tissue and time restrictions prevented all experiments from being repeated. This accounts for some of the absent values in Table 4.1. The other missing data values include the tendon cuts for the Iris scissors. These experiments were not performed for fear of ruining the delicate Iris scissors with the tough tendon. As well, no liver experiments were run in slow speed for the sheep.

1.7.3. *Effects of Sticking.* Another variable which is implicit in the data, but that is not readily distinguishable, is the "stickiness" of the scissors. It was noticed halfway through experimentation that the scissors had become too sticky as a result of the blood drying on the blades. Since the animals are drained before experimentation, they have less blood in the tissues which actually causes the tissues themselves to dry out. Therefore, the doctor periodically sprayed the animal and scissor blades with saline solution.

Stickiness between the blades probably appears in the data as an increase in F_A, but since the spraying was done intermittently when deemed necessary, it is impossible to determine which data files would require a slight correction. This error is not considered

significant for the determination of general trends. However, with another hand present it would have been feasible to wet the scissor and tissue before each cut.

1.7.4. *Hand Orientation.* The angle at which the doctor holds the scissor varied between runs, which resulted in a bias between runs since the force measurement is axis dependent. A better force sensor would be insensitive to the effects of gravity.

Overall, a more accurate description of the tissues and experimental conditions is required for an exact force measure of one tissue type. It is not sufficient to specify simply "skin" or "fascia". The thickness of the tissue and moisture content equally play an important role in the resistance of the tissue and should be measured. As well, future experiments should include more exact tissue preparation and larger sample sizes. With this data, it is only feasible to make general conclusions since many of these variables were neither controlled nor measured.

2. Power Estimation of Signal

The frequency components of the signal were looked at to obtain information about the system. Using Matlab, the power spectral density (PSD) for each signal was determined. Matlab's PSD algorithm uses Welch's method for periodogram averaging. The curves were first segmented into the four phases described in Chapter 3 section 4: (1) opening the scissor, (2) waiting, (3) closing the scissor, and (4) resting before opening again. The PSD of these four phases are shown in Figure 4.6 for each of the three scissors for the cutting of rat muscle. One can see that the signal, for each of the three scissors, has very little high frequency components. These curves are similar for all of the tissue types (skin, liver, tendon, fascia). Most of the frequency components are below 4-5 Hz, typically with a peak between 1.0-3.9 Hz.

Since the cutting action is one smooth closing motion, it is presumed that the 1.0-3.9 Hz components are a property of the tissue being cut. From a modelling point of view, this suggests that only low frequency signals need to be reproduced for realism. Furthermore, this suggests that there must be differences other than the range of the frequency components to explain why the cuts for different tissues feel different. Recall from Chapter 3 section 5 that the Mayo, Metzenbaum and Iris scissors have bandwidths of 102 Hz, 61 Hz and 118 Hz, respectively.

2.0.5. *What makes the tissues feel different?* To investigate this, it is useful to compare some tissue cutting curves, see Figure 4.7. Figures 4.7*a-e* are the blank, muscle, tendon, skin and liver cuts, respectively, for the rat experiments with the Mayo scissors. Looking first at the blank and liver cuts, the closing curves for these runs are relatively smooth, especially compared to the cuts for the muscle and skin in Figures 4.7*b* and *d*. Actually,

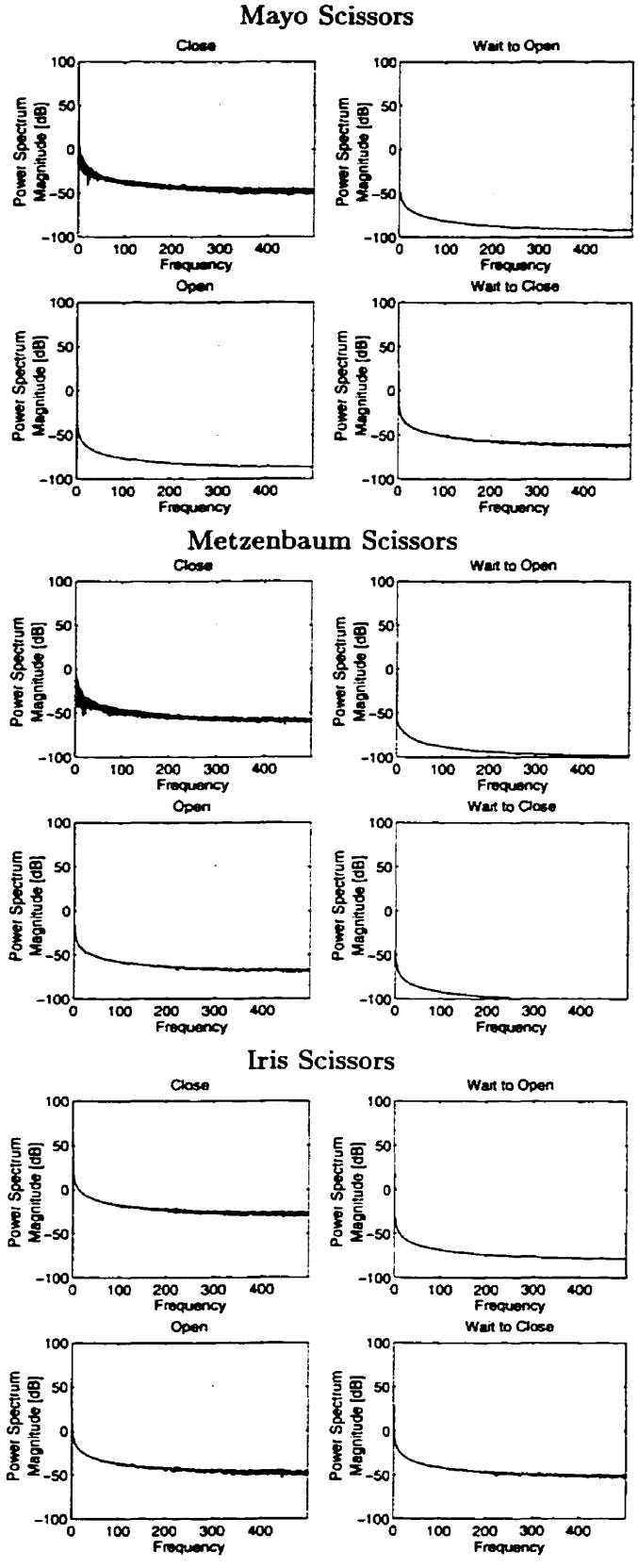

FIGURE 4.6. Power Spectral Density Curves for the force measurements for cutting rat muscle slowly with (*a*) Mayo (*b*) Metzenbaum and (*c*) Iris scissors.

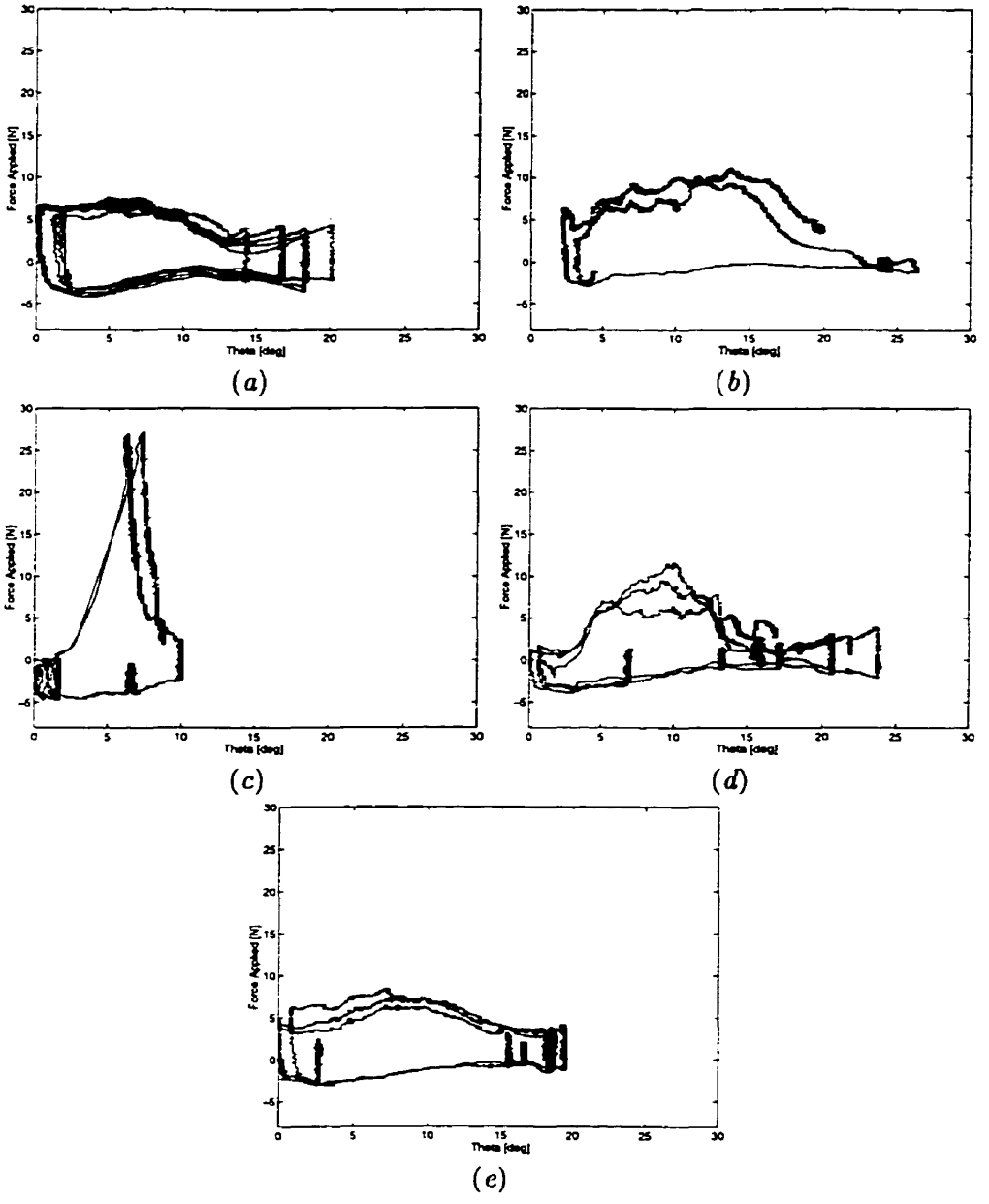

FIGURE 4.7. Comparison of curves for different rat tissue cuts made with the Mayo scissors: (*a*) blank, (*b*) muscle, (*c*) tendon, (*d*) skin and (*e*) liver.

comparing the muscle run to the blank, the differences seem to lie in the magnitude of the force during the closing phase, 6 N for the blank versus 9 N for the muscle, and in the bumpiness, or "texture", of the muscle cut. This distinguishable force magnitude is not present in the skin cuts, however, where the lowest force cut is actually at the level of the blank for the doctor in Figure 4.7*a*, approximately 6 N. When the liver run is compared

to the blank, it seems to be in the same force range as the blank and from this data it is impossible to tell if there truly is a tactile feeling when cutting liver. To test this, blind liver cuts are required since the visual feedback plays an important part on perceived tactile sensation as was pointed out in Chapter 2.

Two possible scenarios could be occurring during the liver cuts. Looking at the total force, it can be broken down into the force required to close the scissor alone, F_{blank}, plus the force to cut the tissue, F_{tissue}, which gives the equation

$$F_{total} = F_{blank} + F_{tissue}. \tag{4.4}$$

One possibility is that the F_{tissue} for liver is negligible and therefore, provides no contribution to the total force of approximately 6 N. The second possibility is that F_{blank} is decreased, say to the student blank force of 4.1 N, due to a lower power grip, which means that the F_{tissue} must contribute approximately 1.9 N in order to bring the total up to the 6 N. A F_{tissue} of 1.9 N is a reasonable estimate since, looking at Table 4.1, the $\max\bar{F}_A$ for rat liver with the Iris is approximately 10.4 N from which must be subtracted the Iris blank $\max\bar{F}_A$, 5 N. This leaves a force of 5 N for the F_{tissue} for the Iris scissors and, as was mentioned, the Iris force is typically 2-3 times the force for the Mayo scissors, this give a range for F_{tissue} of 1.7-2.5 N ($5N/3 = 1.7, 5N/2 = 2.5$). Further experiments with liver would be necessary to verify this result.

Finally, looking at Figure 4.7*c* for the cutting of the tendon, it is clear that this material has a more elastic force profile and the stress increases until breakthrough occurs, with probably little cutting before that point. After the breakthrough, the force drops off rapidly to zero therefore the tactile feedback for this tissue lies in the high force magnitude.

2.1. Texture. The difference felt between rat skin in Figure 4.7*d* and a blank run in 4.7*a* may be strictly in the non-uniformity, or the "texture" felt, rather than a magnitude difference, where this texture is a low frequency texture based on the power spectral analysis.

In order to see if this texture could explain the differences in feel for other samples, the results from the sheep experiments are investigated for the same tissues, see Figure 4.8. One difference which stands out is that for the sheep, the muscle cut seems smoother than the liver, whereas this relationship was opposite for the rat tissues. This could be a result of the fact that the liver for a sheep is much larger in size and actually engulfs the scissor in the tissue as it cuts through it. The sheep skin seems to have a similar texture to the rat skin, however it has a considerably larger force magnitude component, 18 N versus 8 N. This is natural since the sheep skin is much thicker and stronger than the rat skin. The sheep tendon, like the rat tendon, displays a typically elastic-like behaviour where the stress

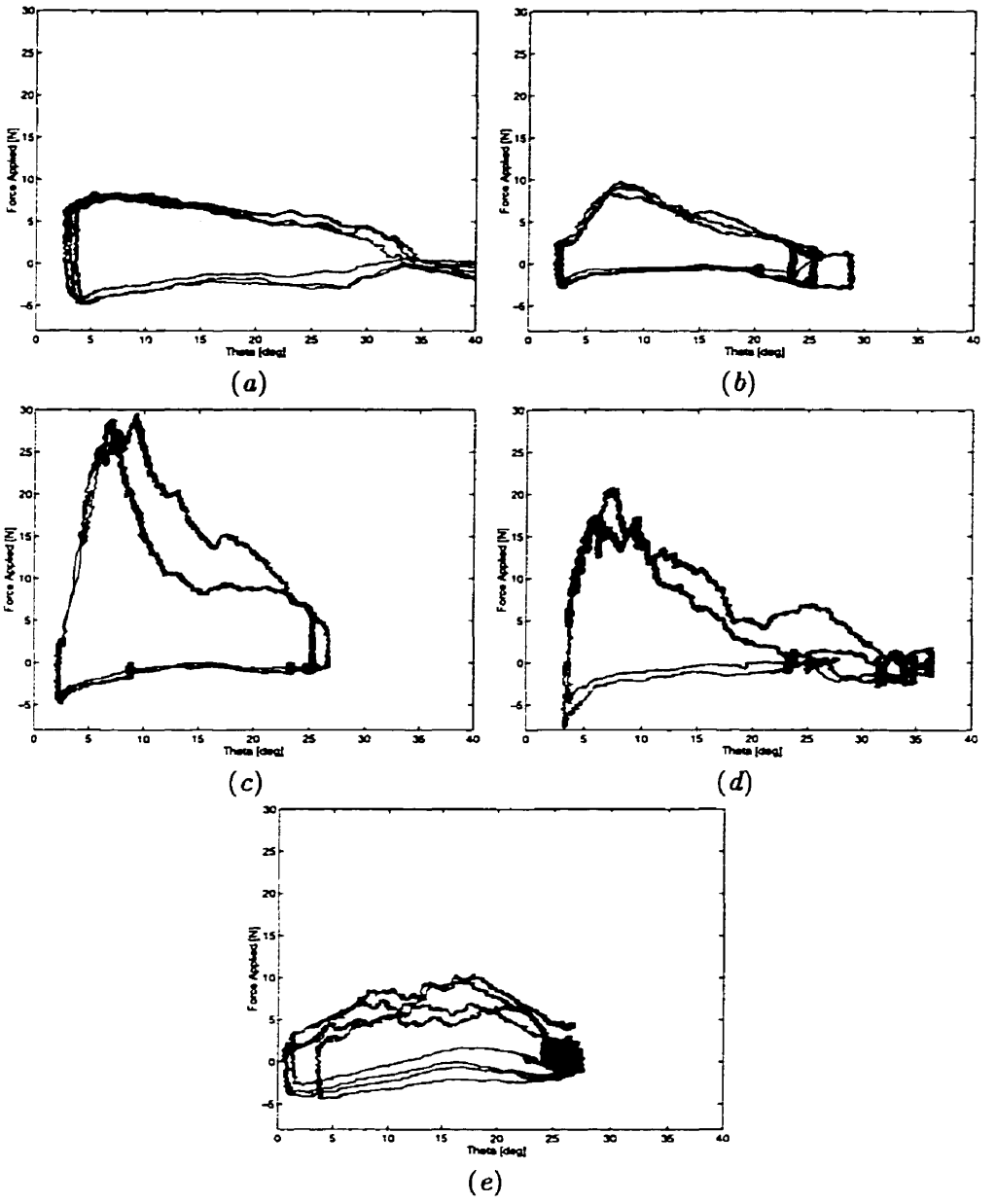

FIGURE 4.8. Comparison of curves for different sheep tissue cuts made with the Mayo scissors: (*a*) blank, (*b*) muscle, (*c*) tendon, (*d*) skin and (*e*) liver.

increases linearly until breakthrough and there is no texture. Therefore, it can be said that some of the tissues like the skin and tendon behave similarly between the rat and sheep for the Mayo scissors. Next, let us compare the Metzenbaum cutting of rat tissues by looking at Figure 4.9.

The same trends are visible for the Metzenbaum cutting of rat tissues as for the Mayo scissors. That is, from Figure 4.9*a*, the blank for the Metzenbaum scissors is relatively smooth, as is the liver cut in Figure 4.9*e*. The tendon cut also involves a steep rise in the force until breakthrough, displaying the same elastic behaviour. Furthermore, the skin and

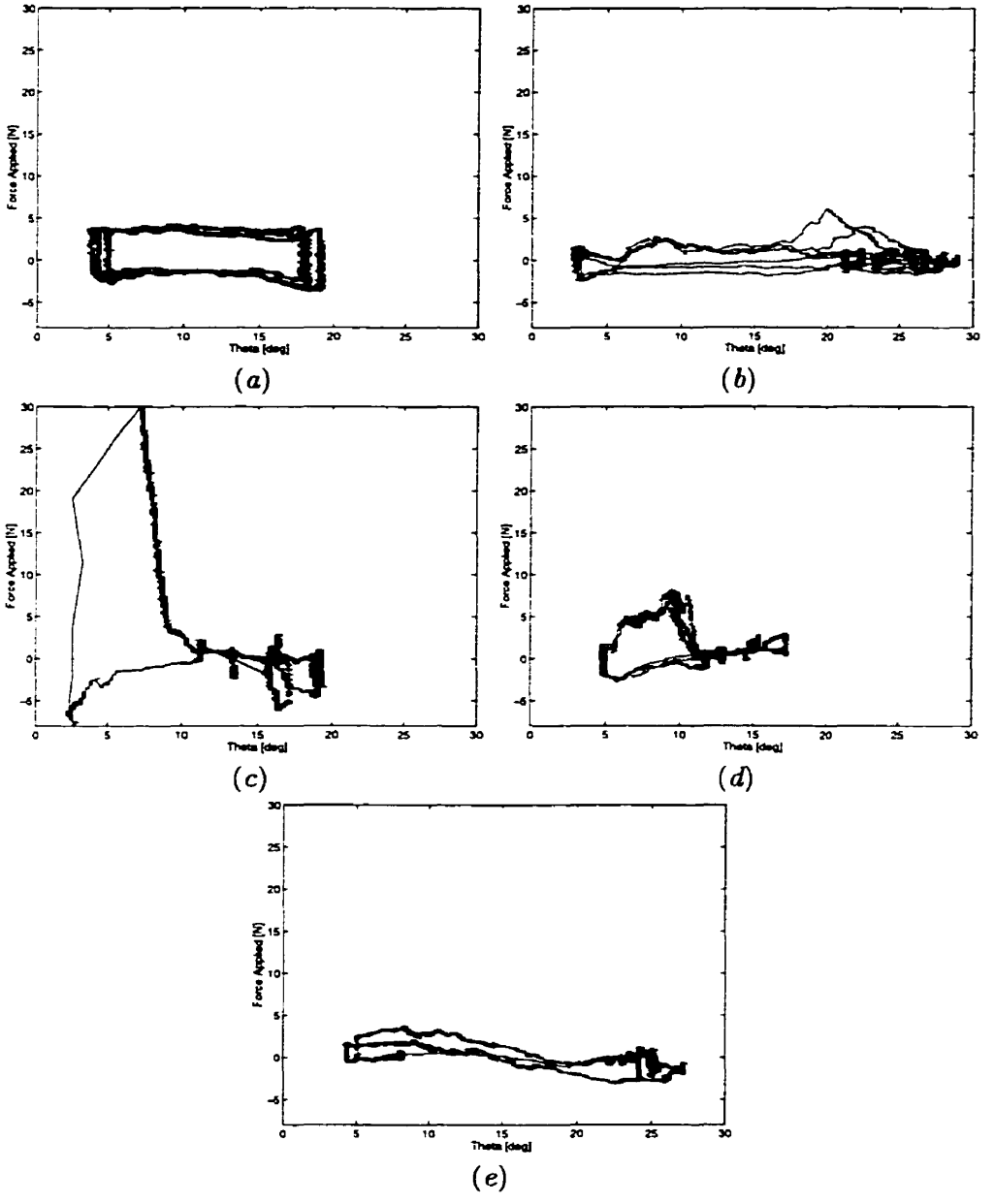

FIGURE 4.9. Comparison of curves for different rat tissue cuts made with the Metzenbaum scissors: (*a*) blank, (*b*) muscle, (*c*) tendon, (*d*) skin and (*e*) liver.

muscle cuts with the Metzenbaum contain textures similar to the ones obtained with the Mayo scissors.

Although all of these sheep trials do not exist for the Metzenbaum cutting of sheep tissues, it can be seen in Figure D.5 in Appendix D that some comparisons are still possible. For the sheep skin cutting with the Metzenbaum scissors, a similar texture to the sheep skin runs with the Mayo scissors can be seen. The fast cutting of fascia with the Metzenbaum closely resembles the Mayo fast cutting of fascia, as well as the liver sheep cut. As with the Mayo, the magnitudes for cutting the sheep tissues are much larger when compared to the rat tissues. For example, the force to cut skin for sheep versus rat is 20 N versus 6 N. As for the Mayo scissors, the liver for the sheep is more textured than the rat liver and required a larger force, 7 N versus 2 N.

Therefore, it seems that the differences in feeling results from the different "textures" of each tissue as well as the magnitude force differences. These textures are not high frequency textures since approximately 99% of the power is in the frequency components below 5 Hz. Recalling from Chapter 3 section 5, the scissors pass all signals below 100 Hz without distortion. This indicates that, a haptic simulation device which used sawed-off surgical instruments as end-effectors would actually only need to provide low frequencies for realism, less than around 5 Hz for the tissue force feedback. This is important due to the haptic feedback device limitations discussed in Chapter 2 section 2.

3. Effect of velocity

3.1. Sum of Squares analysis. It was hypothesised that the force measured is invariant to the velocity, $\dot{\theta}$. To test this, experiments were performed at two speeds, fast and slow, which were determined by the doctor while cutting. It was found that slow corresponds to a speed less than 15 deg/sec with an average of 7 deg/sec and fast is greater than 15 deg/sec with an average speed of 44 deg/sec. However, the average speeds depend on the material being cut. For example, the average fast speed for the blank runs is over 100 deg/sec, whereas the average fast speed for cutting skin is 25 deg/sec.

To determine if the results were significantly different between the two speeds, the sum of squares analysis, described in section 1.6 of this chapter, was used whereas this time, the variability in the slow runs, SSE_S, the fast runs, SSE_F, and the variability between the average slow and fast runs, $\text{SSE}_{S,F}$, were calculated. Again, entire curves are being compared since no accurate model for the closing curve exists. The results of the SSE analysis are presented in Table 4.3.

From Table 4.3 there does not seem to be a statistical significant difference between the slow and fast cutting speeds for any of the Mayo and Metzenbaum experiments. Whereas the

Scissor	Tissue	max(SSE_F, SSE_S)	$SSE_{F,S}$	Statistically different?
Mayo	Blank	1.6	1.1	N
	Skin (sheep, L)	6.0	1.7	N
	Skin (sheep, T)	2.5	1.6	N
	Skin (rat, L)	2.2	0.8	N
	Skin (rat, T)	1.2	0.9	N
	Fascia (sheep)	1.5	1.4	N
	Liver (rat)	1.2	0.8	N
Metz	Blank	1.1	0.9	N
	Skin (sheep, L)	4.9	3.0	N
	Skin (sheep, T)	6.3	4.9	N
	Skin (rat, L)	2.6	1.2	N
	Liver (rat)	1.3	0.6	N
Iris	Blank	2.0	1.2	N
	Skin (sheep, L)	7.8	9.6	Y
	Skin (rat, L)	6.5	5.2	N
	Skin (rat, T)	5.1	5.7	Y
	Fascia (sheep)	6.5	4.5	N
	Liver (rat)	4.1	0.9	Y
	Muscle (sheep)	4.5	10.9	Y

TABLE 4.3. Comparing fast and slow cutting speeds.

experimental results suggest the hypothesis is correct based on the Mayo and Metzenbaum results, the Iris scissors gave a different result. The fast versus slow speed registered as significantly different for the sheep skin cut longitudinally, the rat skin cut longitudinally, the rat liver and the sheep muscle.

Although the Iris results are included only for completeness, it seems premature to draw concrete conclusions about the invariance of the force measure to the velocity. The results for the Mayo and Metzenbaum scissors do strongly indicate this hypothesis however. One possible explanation for the Iris result may be that a speed change incurs a grip change which the smaller, more sensitive Iris scissors are displaying. A more rigorous investigation in the grip effect is needed to determine this.

4. Invariants

Since the tissue experiments introduced many uncontrolled variables, several runs were performed cutting paper in a controlled setting. These runs are presented in Figure 4.10 for the cutting of two and four sheets of 20 lb. standard printer paper. Each graph is composed of more than ten cuts overlapped.

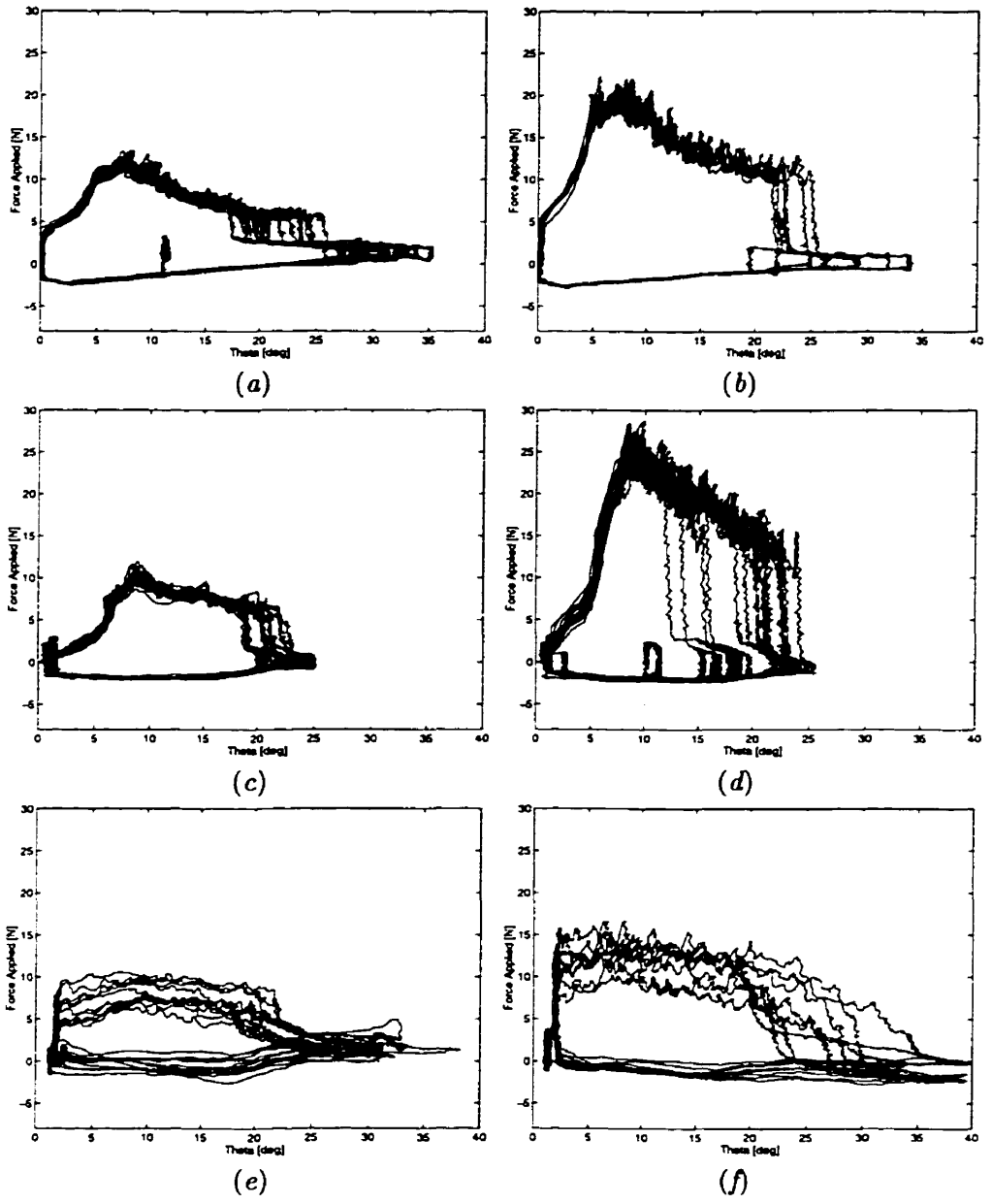

FIGURE 4.10. Cutting of printer paper with Mayo (*a*) two sheets and (*b*) four sheets, with Metz (*c*) two sheets and (*d*) four sheets, and with Iris scissors (*e*) two sheets and (*f*) four sheets.

4.1. Break-through angle. Notice that in Figures 4.10*a* and 4.10*b*, as the Mayo scissor cuts through the paper, the F_A increases until close to 5^o, after which the force drops off. This drop-off for the Metzenbaum scissors, in Figures 4.10*c* and 4.10*d*, is closer to 8^o, whereas this drop-off does not seems to exist for the Iris scissors until the scissor

has fully closed and the cut is finished. This is related to the shape of the blades. Both the Mayo and Metzenbaum have blunt-blunt tips whereas the Iris scissors have pointed tips. Because of this, the Mayo and Metzenbaum scissor blades completely meet before the two handles are closed. For the Iris scissors, however, since the tips are sharp. the blades are not completely closed until the handles are completely together. This phenomena is shown pictorially in Figure 4.11 where in *b*, the Metzenbaum blades have just completely closed as the 8^o opening angle has been reached. Clearly, the Mayo scissors in Figure 4.11*a* will have to close a bit more before the blades completely close against one another, which corresponds to the 5^o mentioned earlier.

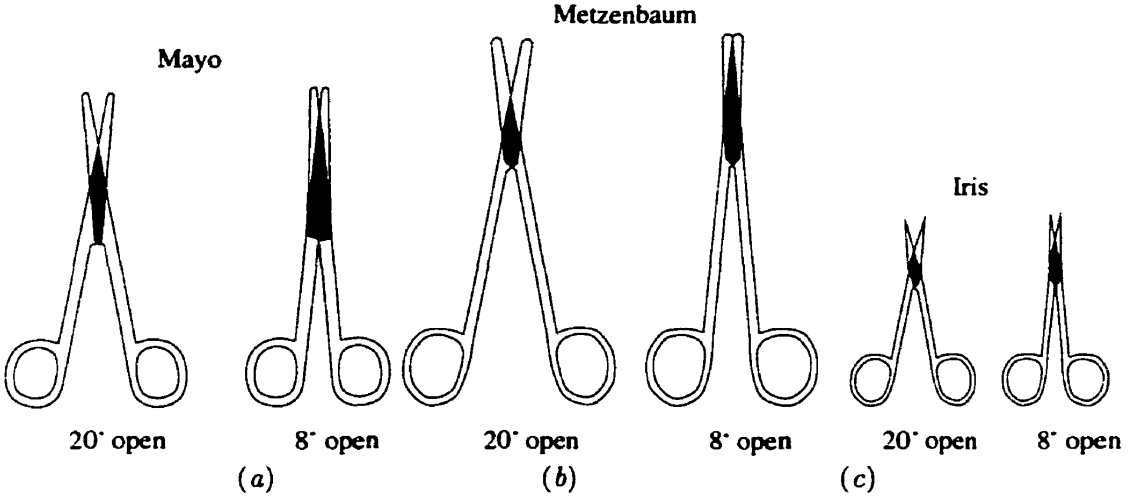

FIGURE 4.11. Different overlap areas for different scissors blade types at same angles θ.

This angle was referred to as the break-through angle, θ_B, in Section 4.1.1 and Table4.1. As can be seen in the table, there are some runs where the max$\tilde{F}_A$ at θ_B data is not available. From Figure 4.7*c* for the tendon, it can be seen that the break-through is not always at this 5^o, however, since the tissue being cut may not be as long as the the length of the blade. From a simulation point of view then, it is important to know the length of the object being cut.

Also depicted in Figure 4.11 are the differences in the contact surface areas between the two blades for the different scissor types at the two angles, 20^o and 8^o. The larger the contact area between the two blades, the higher the force is to overcome the friction. From the figure, it is visible that the Mayo scissors have the largest surface area in contact which may explain why a blank run for the Mayo scissors, as shown in Figure 4.1*b*, requires more force than the other two scissors to open and close. However, equally important, if not more so, is the tightness of the joint screw, which is harder to predict.

One thing to note, in fact, is that depending on the price and manufacturer of the surgical instruments, the empty cut feel is quite different. Distributors of surgical instruments go door-to-door so doctors may choose their instruments by feel. Therefore, it is not sufficient to only specify "Mayo" or "Metzenbaum", for example. The tightness of the screw, the sharpness of the blade edges, the flexibility of the arms vary considerably from scissor to scissor. For these experiments, Piling-Weck's gold handled scissors were selected for their smoothness and sturdy feel.

Returning to the paper cuts, one may expect that the force required to cut four sheets of paper as shown in Figure 4.10*b*, *d* and *f* would require twice as much force as cutting two sheets of paper, Figures 4.10*a*, *c* and *e*. However, this is not so, as determined from the experimental results. For the Mayo scissors, the increase is approximately 1.6 times, for the Metzenbaum approximately 2.5 and for the Iris it is approximately 1.4 times. Clearly, the cutting dynamics are changing and the amount of shearing in front of the contact point is variable. As well, the grip is probably also changing since four sheets of paper are substantially harder to cut through than two.

All of these factors contribute to the difficulty in finding things which are invariant. In general, however, there seems to be a consistent increase in the F_A as the scissor is closing which gives an inversely-proportional relationship between θ and F_A. As well, the slope of the θ-F_A curve seems to be proportional to the maximum of the F_A. For example, the slopes of the curves to cut two sheet of paper for the Mayo and Metzenbaum scissors are approximately -0.48 and -0.33 in Figure 4.10*a* and *c*. The corresponding maximum F_A are approximately 12 N and 10 N. From Figures 4.10*b* and *d*, the slopes of the curves for cutting four sheets of paper are approximately -0.56 and -0.75 and the maximum F_A are 20 N and 25 N for the Mayo and Metzenbaum. Therefore, the scissor with the largest maximum F_A, the Metzenbaum, has the steepest slope.

Also worth mentioning is that the open curves are fairly repeatable. Although the angle at which the doctor stops closing or opening is variable, the behaviour of the F_A between the end-points is fairly constant. As well, the beginning and end of a cut are similar in that they both involve a rapid change in the F_A, but in opposite directions. At the end of a close, the force drops off quickly and at the beginning of a cut, the force rises quickly.

It is important to mention a few observations relating to how a doctor actually uses surgical scissors. One difference between the way a surgeon closes a scissor compared to a non-surgeon is that the doctor will rarely close the scissor completely. Once the feeling of having completely cut through a tissue is reached, the scissor is opened again. This provides a greater feeling of control. As well, a surgeon will not typically use a scissor past 20^o open to make a cut since this results in less control when cutting. Therefore, instead of making

one large cut, many small cuts are made. The only time the scissor is used wide open is when it is used to spread tissues apart, as it is used during tissue preparation. The scissor is often used in this way to isolate different tissue layers.

CHAPTER 5

Conclusions

The forces involved in the cutting of tissues for three surgical scissors were acquired and analysed. Although the experimental method allowed for the determination of general trends in the data, exact quantitative measures for the forces required to cut tissues remain indeterminate. Several improvements to the data acquisition method have been identified and proposed.

1. Limitations and Recommendations

These improvements include eliminating the grip effect from future experimental runs since it inhibits the determination of the innate tissue properties. This may be done either by quantifying it and compensating for it mathematically, or by controlling it, which may require eliminating the human hand from experimentation. The power of the grip, which is a function of the task, and the type of grip, which depends on the contact points between the fingers and the scissor rings, alter the forces measured to cut tissues. At least two grip types have been identified, the pull-open and push-closed grips, but others may exist, especially when the scissor is at rest. The trained surgeon's grip seems to be quite different than the student's, which indicates the necessity to involve a trained surgeon in these experiments at these early stages.

Furthermore, the hand orientation introduced a bias in the force data as the force sensor employed was sensitive to the effect of gravity. An improvement to the force sensor would be to render it axis independent, thereby eliminating this gravity effect. Another possibility is to measure the hand orientation in three space and remove the bias mathematically. However, this method involves further approximations and introduces other sources of error. Therefore, designing a force sensor insensitive to gravity is recommended.

Larger sample sizes are desirable to average out some of the sources of error reviewed above and variabilities between tissue samples. The tissue variability is a result of innate tissue differences from region to region, especially for large tissues such as skin or muscle, and from the varying tissue structures sticking to the tissue of interest. Tissue preparation must be done carefully to obtain the greatest uniformity possible between runs.

Equally important for the determination of the exact forces to cut tissues is the moisture content of the tissue. Due to the blood drying, the tissues and scissor blades were doused intermittently with saline solution, but this event was neither recorded nor accounted for in the data acquisition.

In order to keep track of when the saline solution is applied and the grip changes, as well as measure approximate tissue thickness and visible differences between tissue samples, another person is required in the operating room during experimentation. Since time is limited due to post-mortem effects, video taping the experiments may prove indispensable.

Furthermore, it was determined that the transversal and longitudinal cutting directions may not be necessary for all of the experimental conditions. For example, it was found that the Mayo and Metzenbaum scissors may be insensitive to the fiber directions for skin. For the Iris scissors, however, it remains inconclusive whether the scissor is sensitive to the cutting direction for the skin since the two Iris skin runs do not give the same result. The slow cutting-rate run indicates that there is a significant difference whereas the fast runs do not. Further investigation into the Iris scissors is necessary as they were the hardest to model and provided the most variable results. As for the muscle tissues, both the Mayo and Iris scissors indicate a difference for the two cutting directions. Unfortunately, this result is indeterminable for the Metzenbaum scissors since the data for these trials was not available. Therefore, for the case of Mayo and Metzenbaum scissors on skin it may be possible to reduce the number of experimental conditions, but this is not feasible for the Iris scissor cutting of skin and for the muscle runs. Limiting the data set is especially important as uniform tissue is difficult to obtain. Further experiments into the cutting directions of other tissues, as well as what the Young's modulus may tell us about them, is warranted.

The scissor dynamics themselves are among the factors which influence what the surgeon feels. The length of the scissor arms determines the mechanical advantage which influences the amount of force the user must apply at the handle. The blade characteristics such as edge sharpness, joint screw tightness and degree of curvature change the feel of the scissors. For these reasons, it is important to test the scissors before purchasing them and to determine quantifiable metrics for these parameters.

2. Revisiting Objectives

Although the experimental method would benefit from these improvements, several observations were still possible. First looking at the average maximum force, the measurable differences between tissues include a larger magnitude in the force applied for thicker and stronger tissues. In descending order, forces required to cut the rat tissues were found to be greatest for the tendon, then the muscle, skin, and finally the liver. For the sheep tissues, this order was determined to be tendon, skin, muscle, fascia and finally liver. Although there is a magnitude force difference between tissues, an equally important difference may be in the "texture" of the force versus angle curves. Whereas the liver experiments for the rat and muscle experiments for the sheep are relatively smooth, the skin and fascia curves are more ridged or textured.

This texture consists of only low frequency signal components since approximately 99% of the signal components are below 5Hz as was determined with power spectral density analysis. Whereas 100 Hz would be necessary if the scissors were simulated completely virtually, this is not necessary if the end-effector is a surgical instrument in the real world and only the tissue feedback is simulated. In this case, a force simulator may provide realistic haptics with low bandwidth. For the tendon, however, there is no texture to the curve. The force increases until break-through after which the force drops off quickly. The only haptic feedback seems to be in the force magnitude and elastic behaviour of the material being cut.

By comparing two cutting speeds, the force was found to be independent of the cutting rate for the Mayo and Metzenbaum scissors. Whereas the velocity may not provide information as to what force to expect while cutting, it does indicate the direction of the motion, opening or closing, and when the cutting has stopped, which was useful for the data segmentation. A speed difference may imply a grip change, as is suggested by the Iris velocity analysis results.

Looking into invariants between either tissues or scissors provided the observation that the force required to cut a tissue consistently increases as the scissor angle closes. This may be explained by the squeezing of the tissue which is increased as the θ decreases. As well, the cutting curve is highly repeatable within a run, even if the cutting incident angle varies, which indicates that the tissue force characteristics can be determined with the measured force and scissor angle alone. Other cutting dynamics identified in the data include the shearing of the tissue ahead of the cutting point, the break-through angle and the surface contact area between the blades. Naturally, the degree of shearing is a function of the scissor edge sharpness as well as the tissue properties.

3. Toward Haptic Playback

With the force versus position data acquired, the Freedom-7 Hand Controller will be used to play back these forces. Currently, the haptic device is being equipped with surgical scissor end-effectors for this task. Preliminary trials have been performed to play back these forces on a 2-DOF force feedback device, but the results were inconclusive. The data have been made available on the Internet at: http://www.cim.mcgill.ca /~haptic/tissue/data.html. After the force feedback is provided, a virtual image with modelled tissue properties will be rendered. This final result will provide a step towards the complete realisation of virtual surgery.

APPENDIX A

Basic Dissection Set

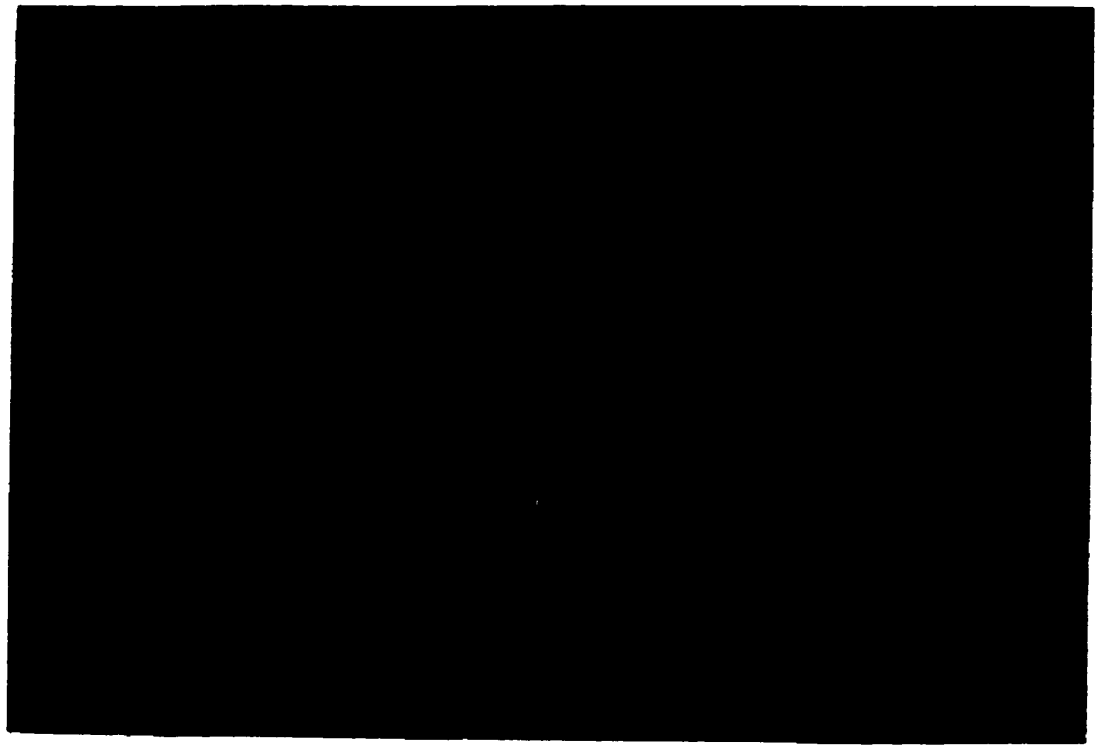

FIGURE A.1. *Left top: top to bottom* 2 Joseph skin hooks, double; 2 Joseph skin hooks, single; *top right,* 1 Mayo dissection scissors, straight; *bottom left to right* 2 Bard Parker Knife handles, No. 3; 2 Adson tissue forceps with teeth (1x2); 2 DeBakey Autraugrip tissue forceps, short; 2 Hayes Martin tissue forceps with multi teeth; 1 Metzenbaum dissection scissor, 5" (12.7 cm); 1 Metzenbaum dissection scissor, 7" (17.8 cm)(Picture from [29])

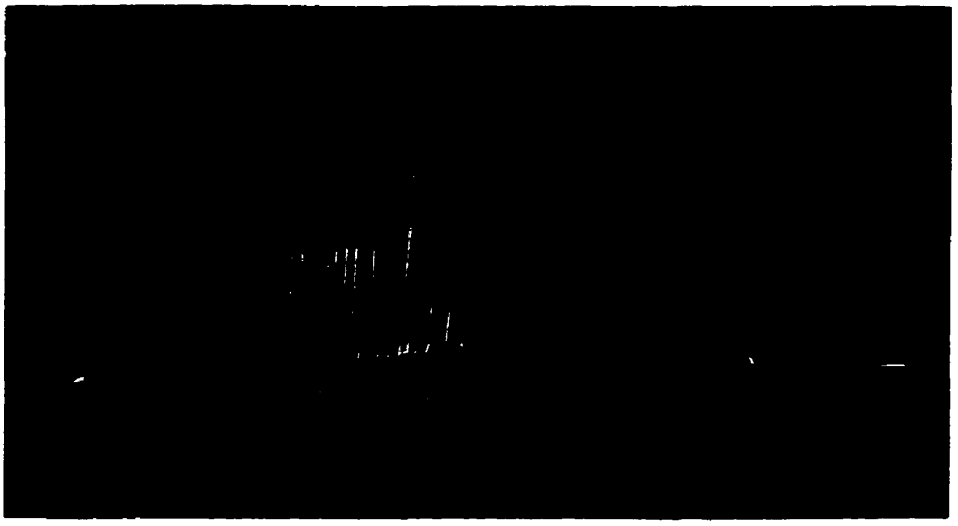

FIGURE A.2. ***Left to right,*** 6 paper drape clips; 6 Halstead mosquito hemostatic forceps, curved; 12 Crile hemostatic forceps, $5\frac{1}{2}$" (14.0 cm) ; 4 Crile hemostatic forceps, $6\frac{1}{2}$" (16.5 cm); 2 Johnson needle holders, 5" (12.7 cm), delicate jaw; 2 Crile Wood needle holders, 7" (17.8 cm); 2 Backhaus towel forceps, small; ***second instrument stringer:*** 2 Allis tissue forceps, short; 8 Adair breast forceps; 4 hemostatic tonsil forceps. (Picture from [29])

FIGURE A.3. ***Left to right,*** 2 Miller-Senn retractors; 2 Volkmann retractors, 4 prong, sharp; 2 Army Navy retractors; 2 Richardson retractors: small, medium. (Picture from [29])

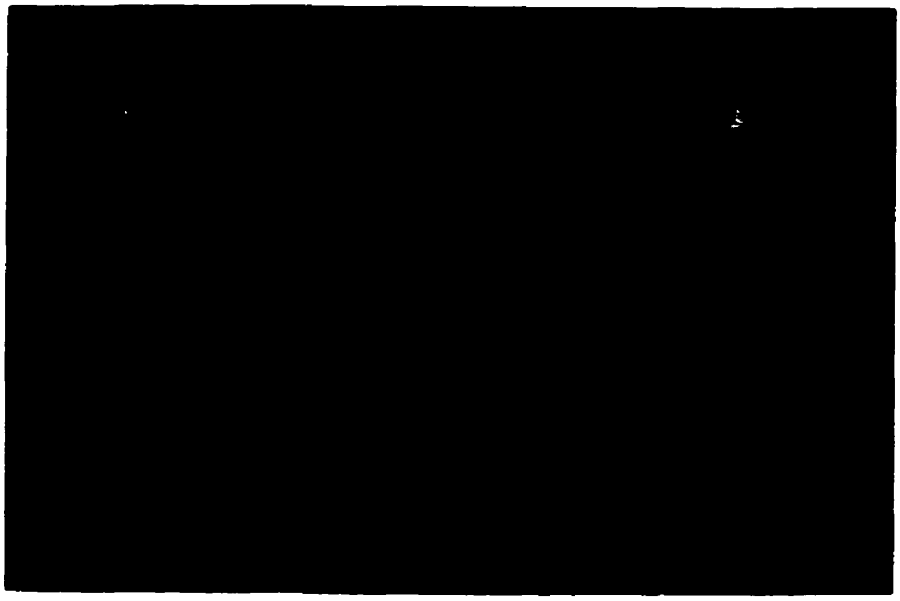

FIGURE A.4. *Top to bottom,* 1 Yankauer suction tube with tip; 1 stylet; 1 Baron suction tube with finger valve control; 2 Weitlaner retractors, straight. (Picture from [29])

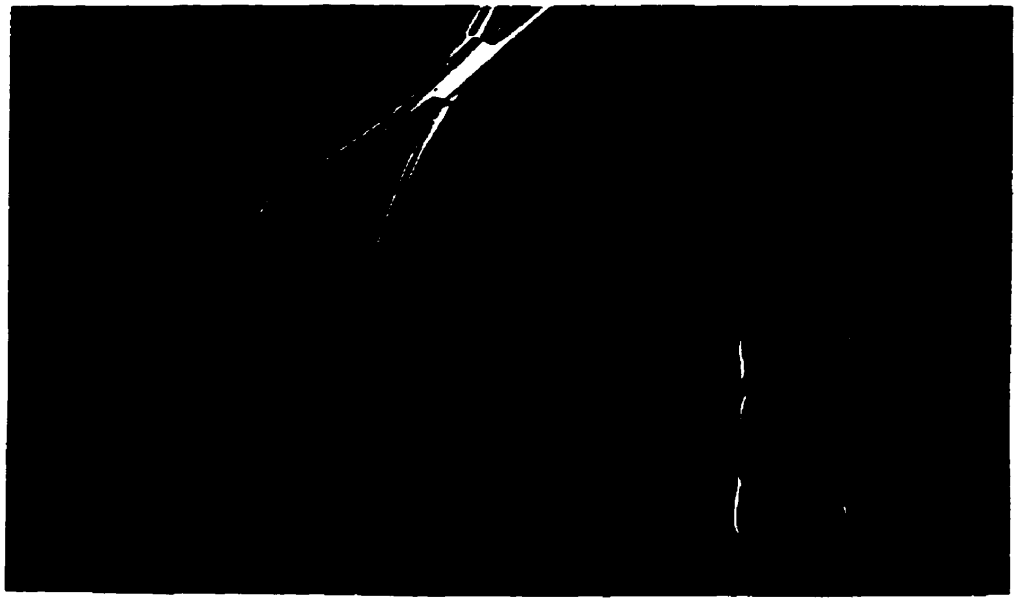

FIGURE A.5. Adair breast forceps: tip and front view. (Picture from [29])

APPENDIX B

Skin Characteristics

A brief description of the skin is provided since it is the surface which is essentially the true force sensor [22]. The skin is a system of layers. On the top there is the epidermis, below which is the the dermis (or corium) which contains the nerve endings which are both encapsulated or free, below which is the reticulated dermis and below all of that is the subcutaneous tissue.

The Receptors. Glabrous and hairy skin have different mechanoreceptors located in the skin. The receptors in hairy skin are:

- hair follicle receptors are basket endings which surround the follicles
- the Merkel's disk which are near the hairs
- Ruffini endings are spindle shaped capsules
- Pacinian corpuscles
- C-mechanoreceptors which are free-nerve endings.

The glabrous skin, encapsulated receptors are

- Meissner's corpuscles
- Merkel receptor complexes
- Ruffini endings
- Pascinian corpuscles
- free-nerve endings (not encapsulated).

Classification and Descriptions. Receptors fall into two categories: *rapidly adapting* and *slowly adapting.* Rapidly adapting receptors are the Pacinian corpuscles and the Meissner corpuscles. The slowly adapting receptors are the Merkel's cells, Ruffini endings and C-mechanoreceptors.

The Pacinian corpuscles are vibration receptors and acceleration-sensitive. They are sensitive to pressure and respond to vibration but not to direction. They have a maximum detection threshold at a rate near 30 Hz and a minimum threshold between 250-300 Hz. Above 300 Hz, the detection threshold increases again.

The Meissner's corpuscles adapt a bit slower then the Pacinian with discharge ceasing after 50-500 milliseconds. They are velocity-sensitive mechanoreceptors that discharge only when the skin is moving. They fire only for stimulations between 10-100 Hz.

Slowly adapting receptors continue to fire even when the pressure is maintained for a long time. The two types of slowly adapting mechanoreceptors are the SA I and SA II. SA I units respond at high frequencies and fire impulses at an irregular rate. SA II units respond to stretching of the skin and fire impulses at a regular rate.

The Merkel's cells are SA I units which respond to compression and shear stimuli whereas Ruffini endings are SA II units and provide a continuous indication of pressure or tension in the skin.

The C-mechanoreceptors fire slowly-adapting discharge for skin indentation or hair movements but do not respond to repetitive excitation.

These receptors are distributed unevenly over the hand. B.1

Thresholds for Sensation. At low frequencies, between 20 to 40 Hz, the contact area size seems to have no affect on the threshold of feeling. However, at high frequencies, over 200, the contact area does play an important role. However, the curves remain U-shaped with minimum threshold about 250-300 Hz.

The lower limit to the sensation of vibration is around 10 to 80 Hz and the upper limit as cited in [18] as 8192 Hz. However, the ability to discriminate one signal from the other declines above 320 Hz.

The Kinesthetic Sense. Kinesthetics usually refers to the sensation of movement, but in this section it will refer also to the sensation of static position and sensations arising from the contractions of the muscles.

There are various mechanoreceptors which provide the static and moving sensations. The two broad classes of inputs are position (or displacement) signals which give continuous joint angle information and movement (or transient) signals which are available only during movement. Relatively little is certain about which receptors are involved in the detection of movement. However, since the contact between hand and surgical instrument is mostly static, the movement receptors are of little interest in this work.

The sense of position is more well known. Three possible sources of Kinesthetic sensory information are mechanoreceptors in the skin, mechanoreceptors in the joints and

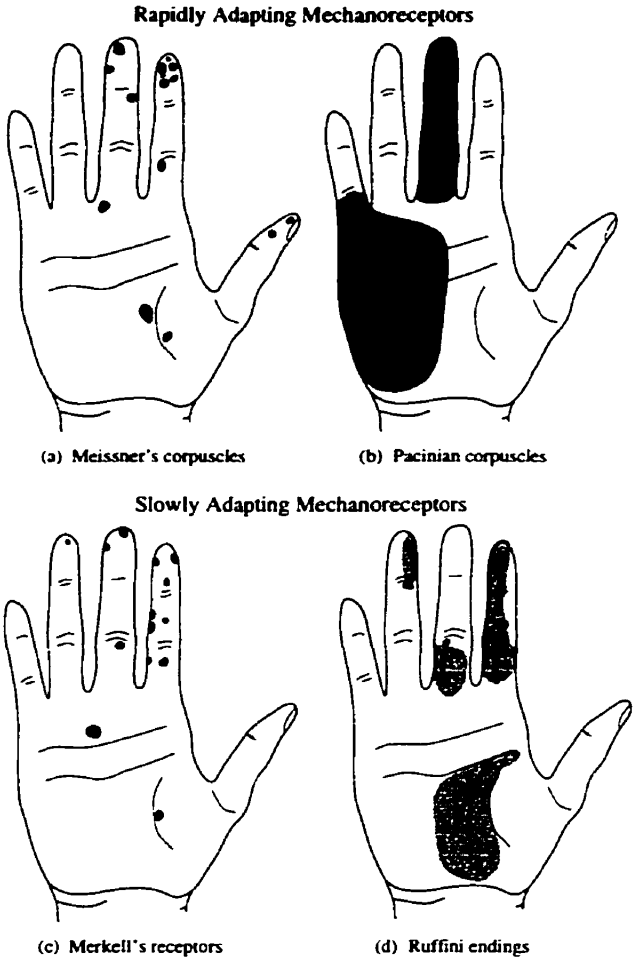

FIGURE B.1. Receptive filed in the inner surface of the hand

mechanoreceptors in the muscles. The mechanoreceptors in the skin have been reviewed above. The mechanoreceptors in the joint are numerous slowly adapting such as the Golgi tendon organs and the Ruffini type endings. The Golgi tendon organs are also found in the muscles where they are in series with the muscles and measure the tension of the muscle. Parallel to the main muscle fibers are the muscle spindle mechanoreceptors. They measure the length and rate of change of length of the fibers.

The Golgi tendon organs and the muscle spindles are able to discharge responses at rates up to 300 Hz, however, it is clear that the reception of the stimuli is slower than this. It is likely that the central nervous system integrates the impulses to obtain a more accurate average. Therefore, movements played back on the force-feedback device need be no higher than 300 Hz, and quite possibly even lower.

APPENDIX C

Semiconductor Strain Gauge Installation

Applying the Strain Gauges. The manufacturer's instructions were modified slightly because it was found to be more suitable to this application:

(i) Lightly sand with 400 grit sandpaper, perpendicular to the strain dimension, to a 16 μinch rms finish, sandblast to a matt surface.

(ii) Apply 1,1,1-trichloroethane to clean the surface.

(iii) Blow dry with canned air or another clean source.

(iv) Clean with acetone.

(v) Blow dry with canned air or another clean source.

(vi) With a fine brush (000), precoat with thin layer of epoxy (Micro-Measurement's M-bond 610). The precoat is to establish electrical isolation.

(vii) Air dry the precoat for 1/2 hour at ambient temperature.

(viii) Cure for 1/2 to 1 hour at $90°C$.

(ix) Repeat precoat procedure (steps 6, 7 and 8).

(x) Remove the gauge from the package. This must be done with a lot of care because the tape is very sticky. Holding the free end of one lead wire with a fine tweezer, remove the wire from the tape by gently lifting the wire straight up. Be sure that the lead is completely free from the tape before going on to the second lead. Gently remove the second lead wire.

(xi) Place the gauge on the wet epoxy and align.

(xii) Overcoat the gauge with a thin layer of epoxy.

(xiii) Air dry for 1/2 hour at ambient temperature. Ensure that the surface is completely flat because the gauge will otherwise slip. Check periodically during the half hour to ensure that the gauge is still aligned.

(xiv) Cure at $125°C$ for 12 hours.

Soldering Instructions: Do not contact the lead wire with the soldering iron, it will evaporate.

(i) Tin the end of the connection wire.

(ii) Place a ball of solder on the solder pad.

(iii) Extend the connection wire beyond the solder pad and lightly touch the lead wire against the connection wire.

(iv) Quickly solder the connection wire by contacting the soldering iron only as far as the solder pad. Do not leave the soldering iron an the connection wire any longer than necessary.

Note: The lead wire will heat up enough to bond to the connection wire even without the soldering iron ever touching it.

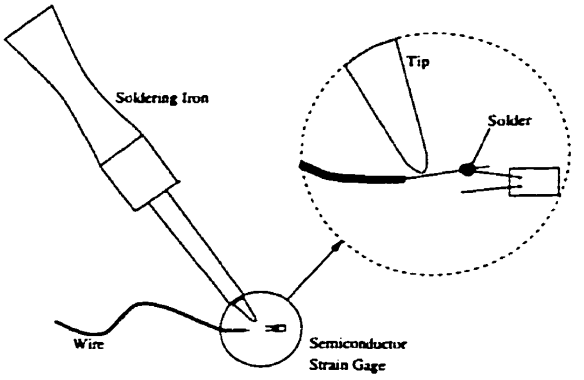

FIGURE C.1. Soldering instructions for semiconductor strain gauges.

APPENDIX D

Experimental Force Curves

In the following pages, the experimental data is presented. The data is obtainable in ASCII format from the internet. This address is http://www.cim.mcgill.ca/~haptic/tissue/data.html. Some curves have two cuts overlapped, some have as many as fifteen cuts. The data is downloadable by simply selecting the figure of interest.

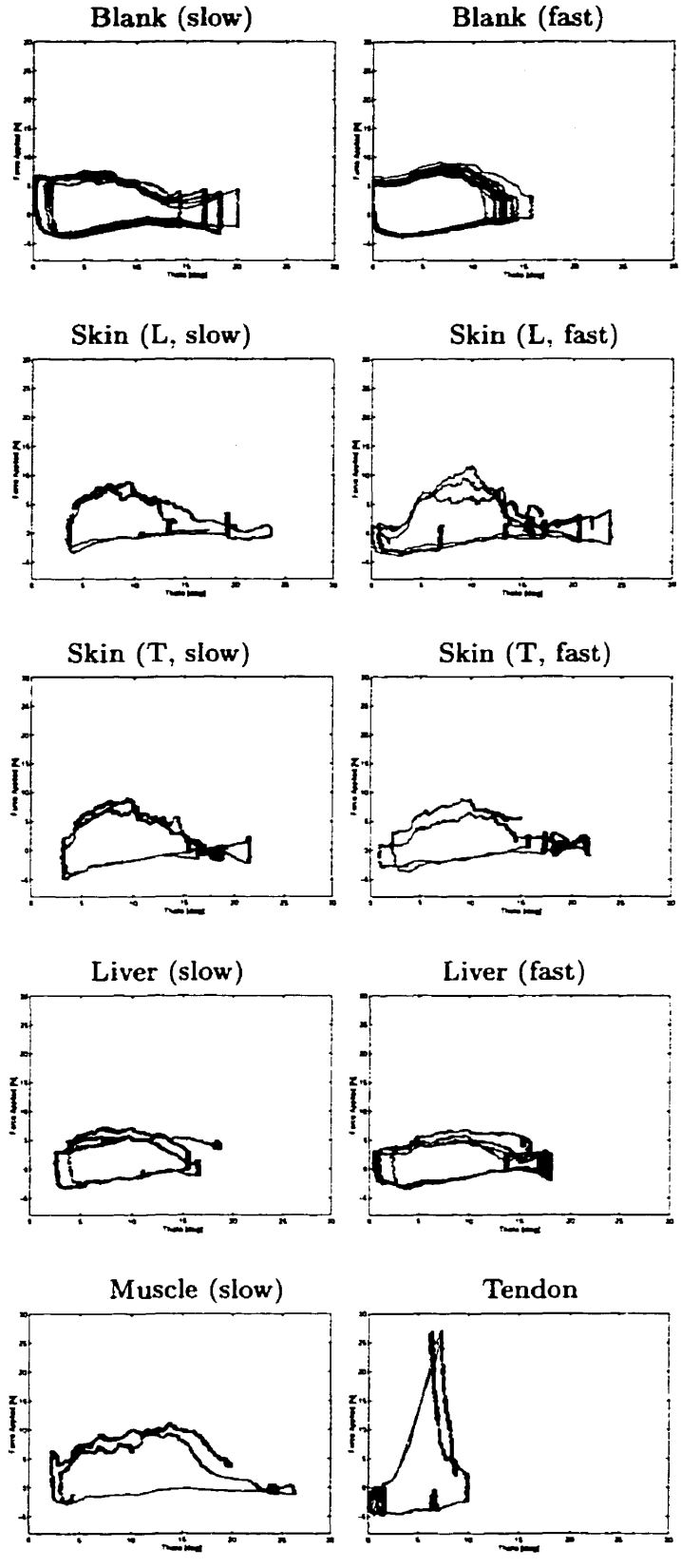

FIGURE D.1. Force applied versus angle θ for the cutting of various rat tissues with Mayo scissors.

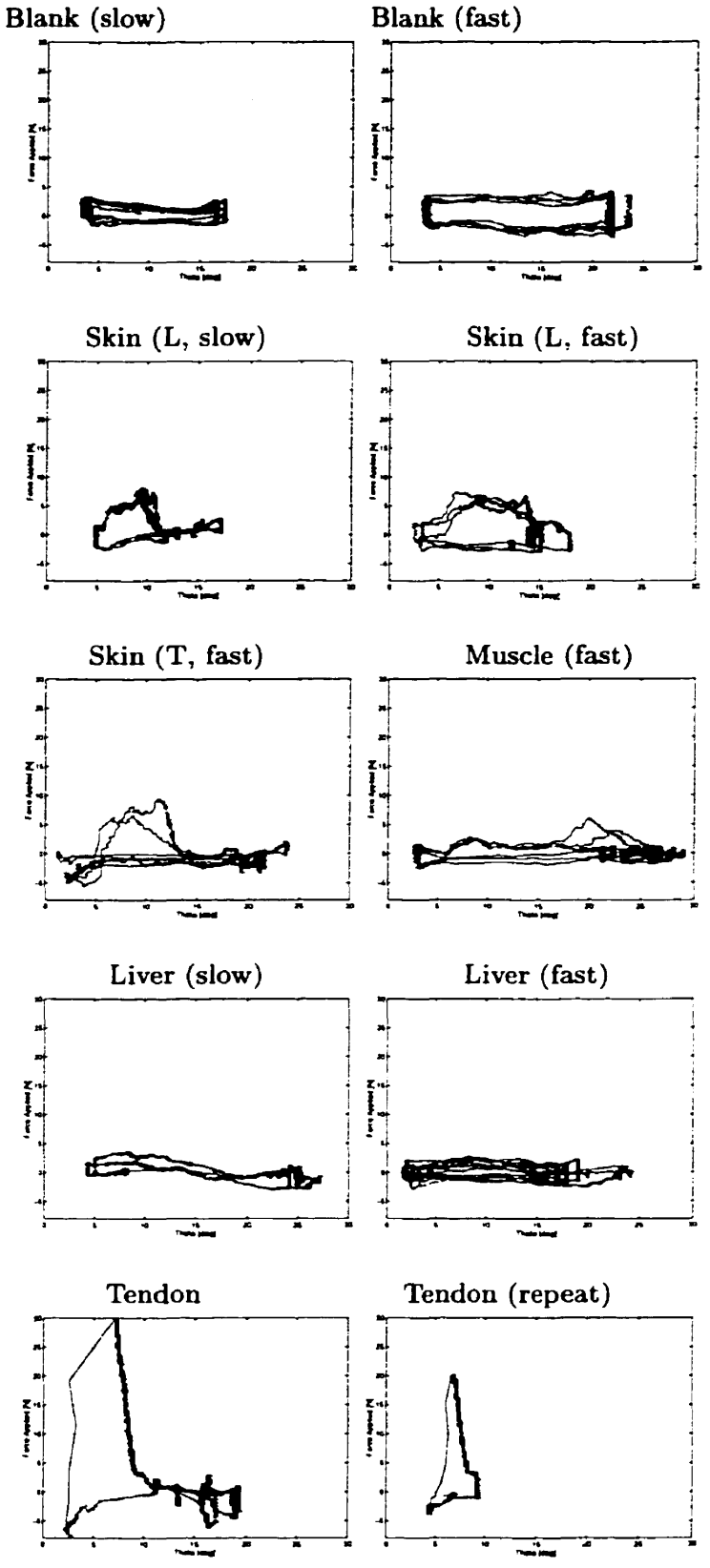

FIGURE D.2. Force applied versus angle θ for the cutting of various rat tissues with Metzenbaum scissors.

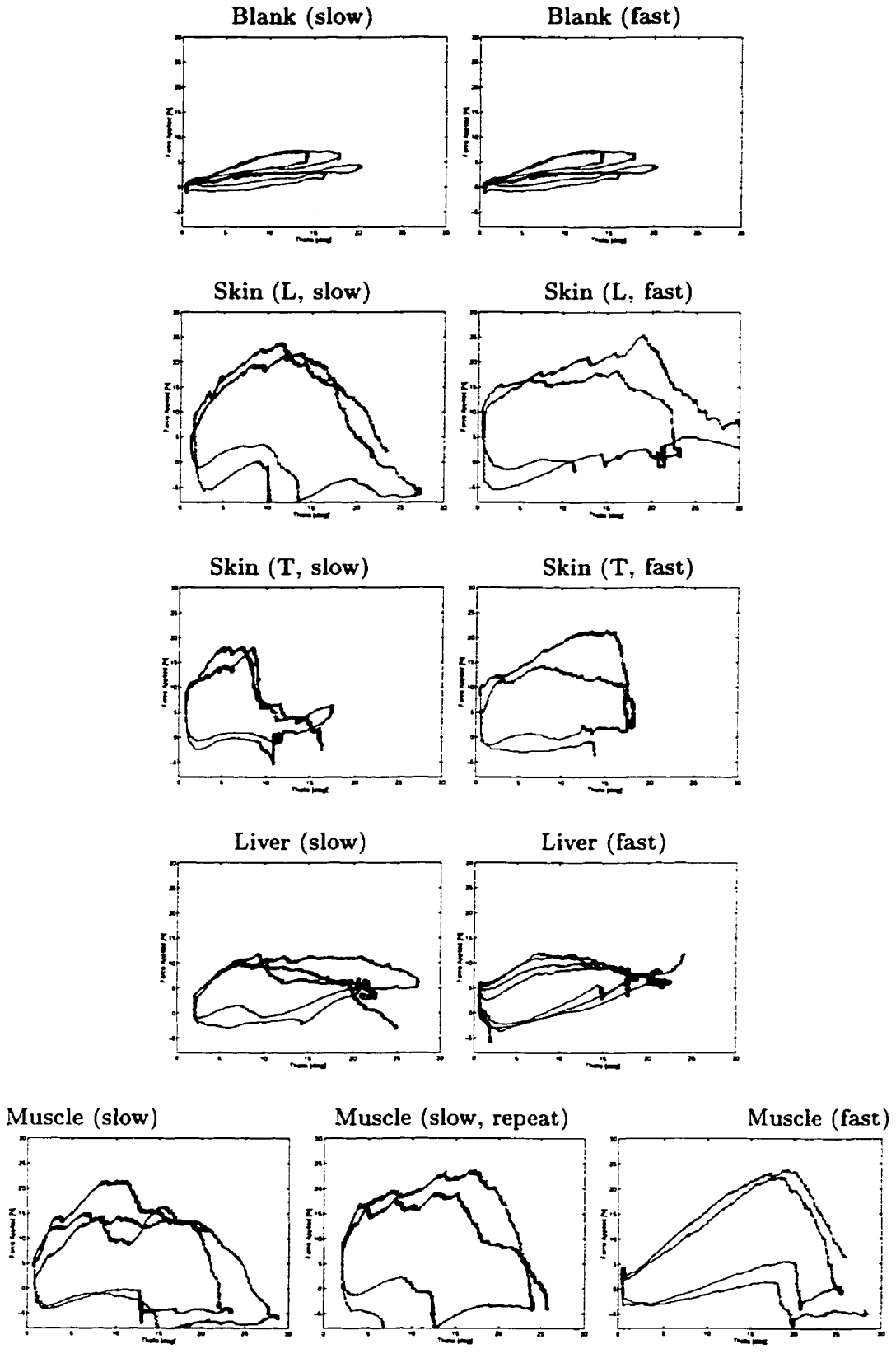

FIGURE D.3. Force applied versus angle θ for the cutting of various rat tissues with Iris scissors.

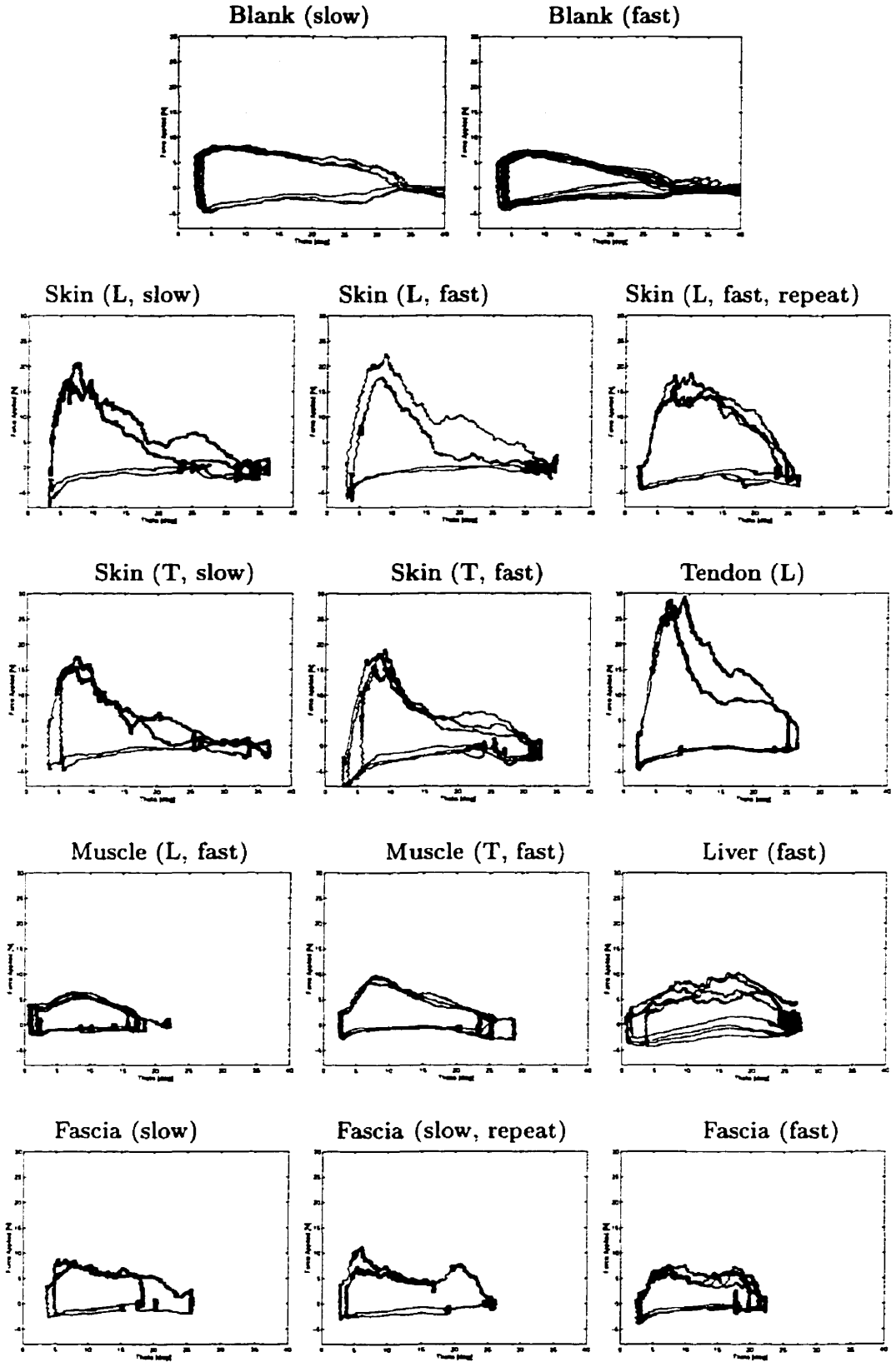

FIGURE D.4. Force applied versus angle θ for the cutting of various sheep tissues with Mayo scissors.

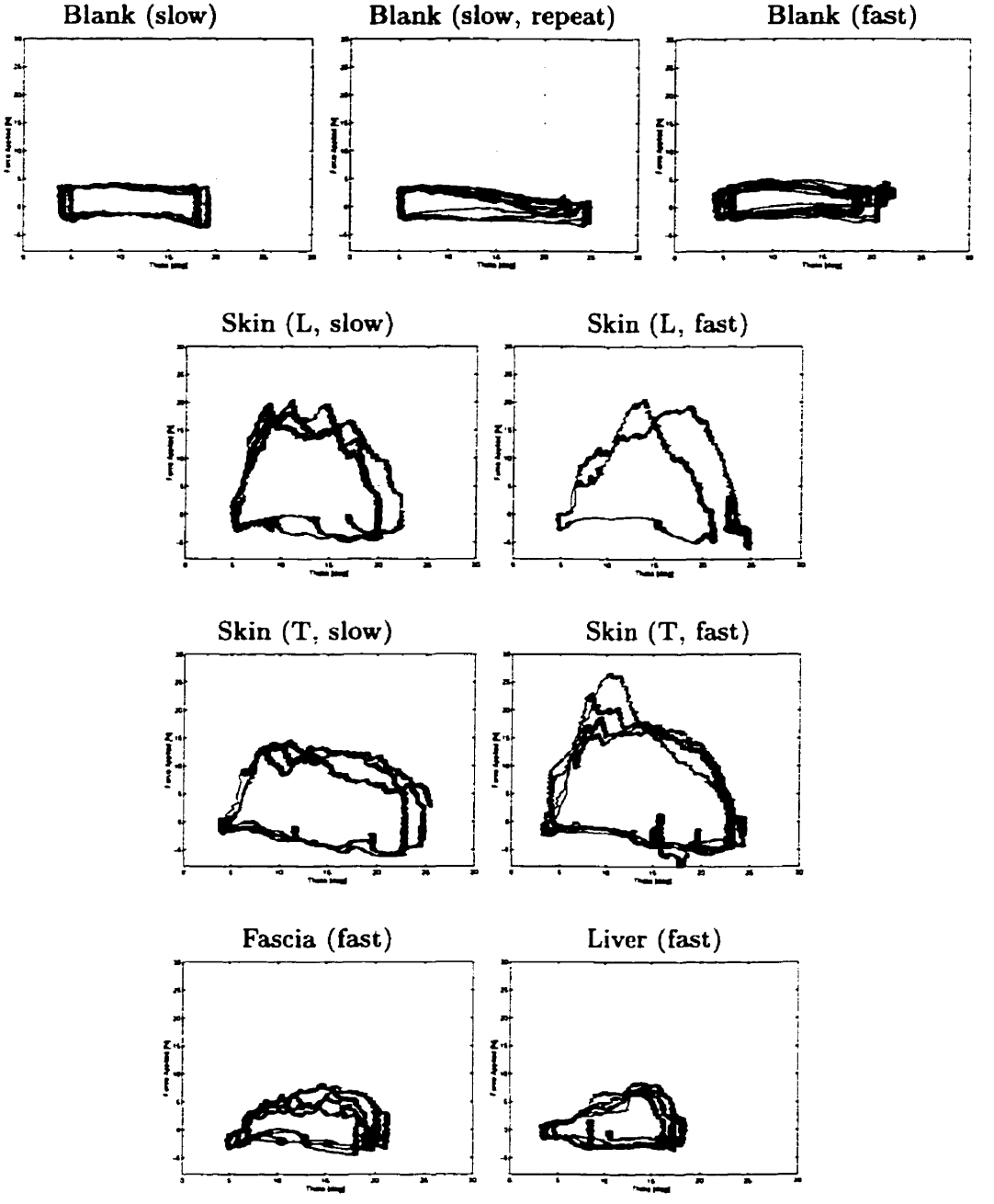

FIGURE D.5. Force applied versus angle θ for the cutting of various sheep tissues with Metzenbaum scissors.

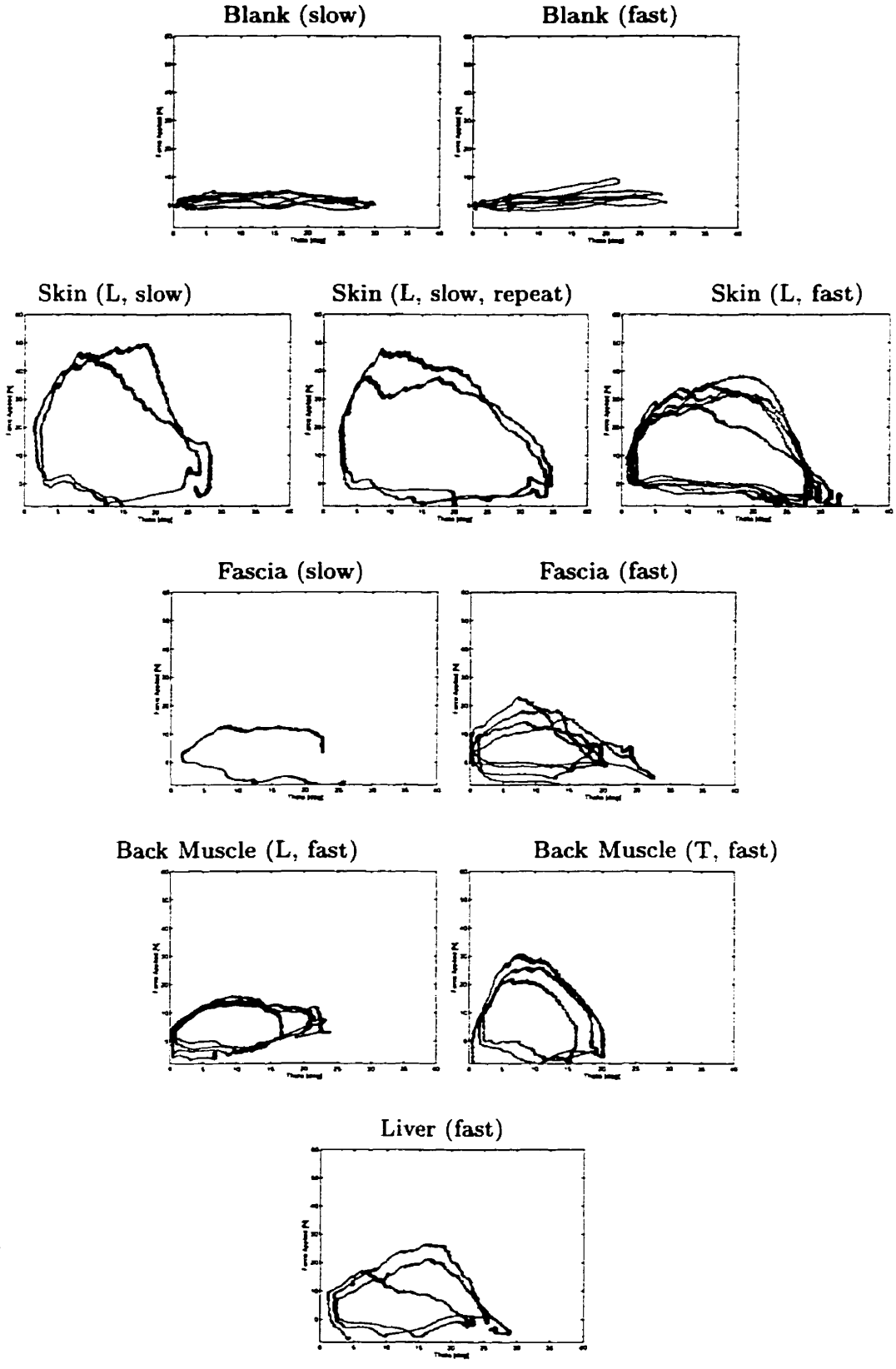

FIGURE D.6. Force applied versus angle θ for the cutting of various sheep tissues with Iris scissors.

APPENDIX E

Grasp Taxonomy

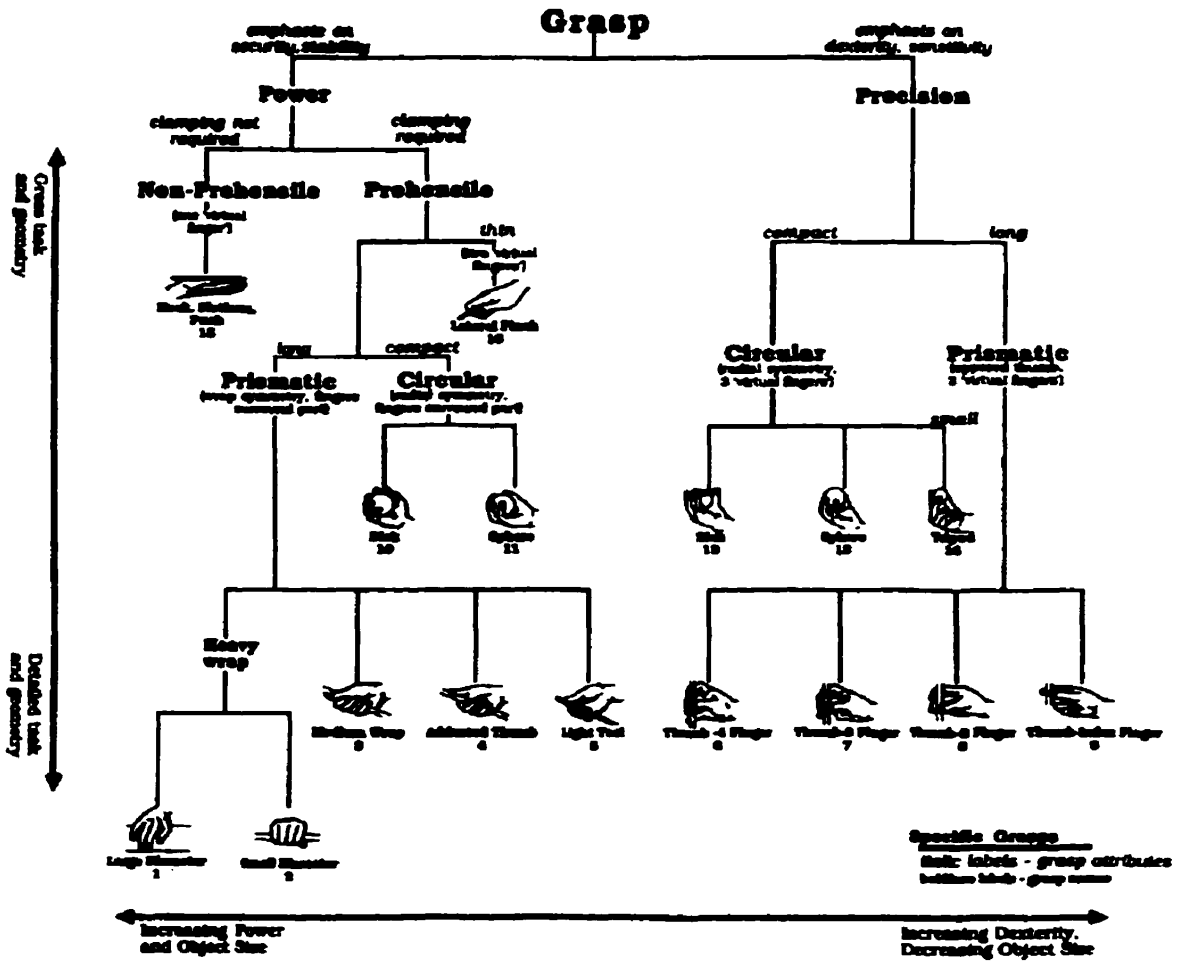

FIGURE E.1. A partial grasp taxonomy of manufacturing grasps, as modified by Cutkosky. (Picture from [4])

APPENDIX F

Handling the Instruments

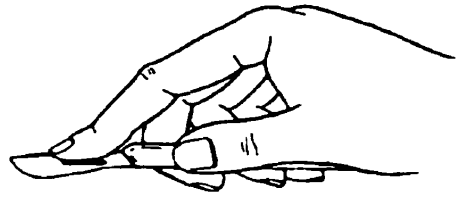

FIGURE F.1. Holding the scalpel for cutting skin. (Picture from [19])

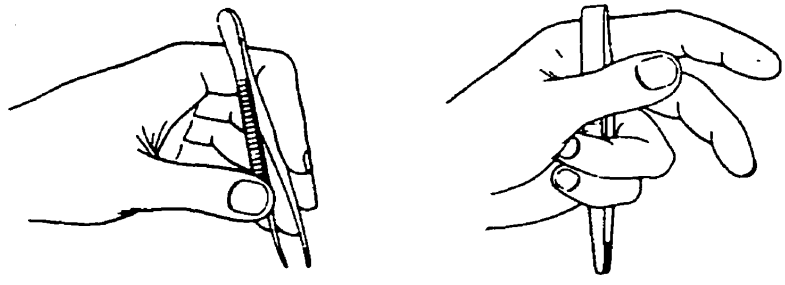

(*a*) (*b*)

FIGURE F.2. (*a*) Gripping dissecting forceps. Notice that the left hand is being used. (*b*) Palming the dissecting forceps to free the thumb, index and middle fingers. (Picture from [19])

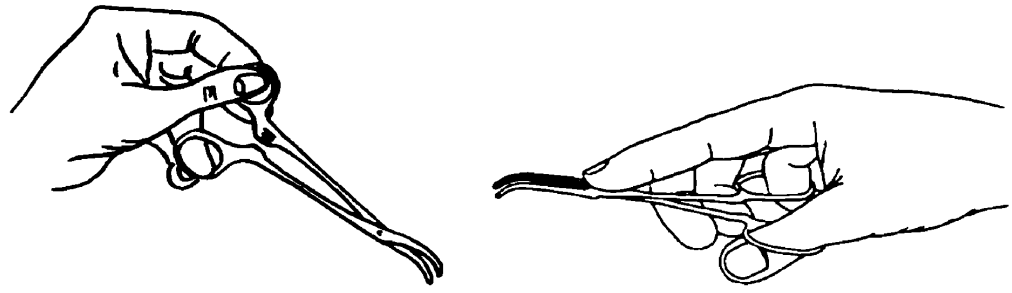

(*a*) (*b*)

FIGURE F.3. (*a*) Applying artery forceps. (*b*) Removing artery forceps with the left hand. (Picture from [19])

REFERENCES

[1] M. J. Ackerman. The visible human project. In *Medicine meets virtual reality II: Interaction technology and healthcare*, pages 5–7, Washington, D. C., 1994. IOS Press.

[2] E. Bainville, P. Chaffanjon, and P. Cinquin. Computer generated visual assistance during retroperitoneoscopy. *Computers in Biology and Medicine*, 25(2):165–171, 1995.

[3] C.W. Burckhardt, P. Flury, and D. Glauser. Stereotactic brain surgery. *IEEE Engineering in Medicine and Biology*, pages 314–317, May/June 1995.

[4] M. R. Cutkosky. On grasp choice, grasp models and the design of hands for manufacturing tasks. *IEEE Journal of Robotics and Automation*, 5(3):269–279, June 1989.

[5] S. Delp, P. Loan, C. Basdogan, and J. Rosen. Surgical simulation: An emerging technology for training in emergency medicine. *Presence*, 6(2):147–159, April 1997.

[6] Francis A. Duck. *Physical Properties of Tissue*. Academic Press, 1990.

[7] A. Dumay and G. Jense. Endoscopic surgery simulation in a virtual environment. *Computers in Biology and Medicine*, 25(2):139–148, 1995.

[8] S. Lavallée et al. Image guided operating robot: A clinical application in stereotactic neurosurgery. In *Proceedings IEEE Int. Conf. on Robotics & Automation*, pages 618–624, Nice, France, May 1992.

[9] G. Faulkner and M. Krauss. Guidelines for establishing a virtual reality lab. *IEEE Engineering in Medicine and Biology*, pages 86–93, March/April 1996.

[10] Y. C. Fung. *Biomechanics*. Springer-Verlag, 2 edition, 1993.

[11] D. Glauser, P. Flury, and C. W. Buckhardt. Mechanical concept of the neurosurgical robot 'minerva'. *Robotica*, 11(6):567–575, Nov/Dec 1993.

[12] P.S. Green, J.W. Hill, J.F. Jensen, and A. Shah. Telepresence surgery. *IEEE Engineering in Medicine and Biology*, May/June 1995.

[13] P.S. Green, J.F. Jensen, J.W. Hill, and A. Shah. Mobile telepresence surgery. Technical report, SRI International, 1995.

[14] V. Hayward, P. Gregorio, O. Astley, S. Greenish, M. Doyon, L. Lessard, J. McDougall, I. Sinclaire, S. Boelen, X. Chen, J.-P. Demers, J. Poulin, I. Benguigui, n. Almey, B. Makuc, and X. Zhang. Freedom-7: A high fidelity seven axis haptic device with applications to surgical training. In *5th International Symposium on Experimental Robotics*, Barcelona, Spain, June 1997.

[15] V. Hayward, F. Janabi-Sharifi, and J. Chen. Adaptive windowing discrete-time velocity estimation techniques: Application to haptic interfaces. In *Symposium on Robotic Control SYROCO*, 1997.

[16] I. Hunter, L. Jones, M. Sagar, S. Lafontaine, and P. Hunter. Opthalmic microsurgical robot and associated virtual environments. *Computers in Biology and Medicine*, 25(2):173–182, 1995.

[17] P. Kazanzides, J. Zuhars, B. Mittelstadt, and R. Taylor. Force sensing and control for a surgical robot. In *IEEE Robotics & Automation Conference*, pages 612–617, Nice, France, May 1992.

[18] Dan R. Kenshalo. *Handbook of Perception: Feeling and Hurting (Vi-B)*, chapter Tactile sensitivity, pages 30–49. Academic Press, 1978.

[19] R.M. Kirk. *Basic Surgical Techniques*. Churchhill Livingstone, 1978.

[20] K. E. MacLean. The haptic camera: A technique for characterizing and playing back haptic properties of real environments. In *ASME Dynamics Systems and Control Division*, volume 58, pages 459–467, 1996.

[21] Prem S. Mann. *Introductory Statistics*, chapter 13. John Wiley & Sons, Inc., 3 edition, 1998.

[22] F. Reynier and V. Hayward. Summary of the kinesthetic and tactile function of the human upper extremities. Technical report, CIM, 1993.

[23] J. Rosen, A. Lasko-Harvill, and R. Satava. Virtual reality and surgery. In *Computer-Integrated Surgery: Technology and Clinical Applications*, chapter 14, pages 231–242. MIT Press, 1996.

[24] R. Satava and S. Jones. An integrated medical virtual reality program. *IEEE Engineering in Medicine and Biology*, pages 94–97, March/April 1996.

[25] R. M. Satava and S. B. Jones. Virtual environments for medical training and education. *Presence*, 6(2):139–146, April 1997.

[26] Richard M. Satava. Virtual reality and telepresence for military medicine. *Computers in Biology and Medicine*, 25(2):229–236, 1995.

[27] T. Sheridan. Human factors in telesurgery. In *Computer-Integrated Surgery: Technology and Clinical Applications*, chapter 13, pages 223–229. MIT Press, 1996.

[28] M. A. Srinivasan, G. L. Beauregard, and D. L. Brock. The impact of visual information on the haptic perception of stiffness in virtual environments. In *Proceedings of the ASME Dynamics Systems and Control Division*, volume DSC-Vol. 58, pages 555–559. ASME, 1996.

[29] S. M. Brooks Tighe. *Instrumentation for the Operating Room.* Mosby, 4th edition, 1994.

[30] L. J. Vroomen. Measurement laboratory: Lecture notes. Technical report, McGill University, 1997.

[31] R. Ziegler, G. Fischer, W. Mueller, and M. Goebel. Virtual reality anthroscopy training simulator. *Computers in Biology & Medicine*, 25(2):193–293, 1995.

[32] O. C. Zienkiewicz. *The Finite Element Method*, chapter 18. McGraw-Hill, 3 edition, 1977.

Document Log:

Manuscript Version 0
Typeset by $\mathcal{A}\mathcal{M}\mathcal{S}$-LaTeX — 7 October 1998

STEPHANIE GREENISH

CENTER FOR INTELLIGENT MACHINES, MCGILL UNIVERSITY, 3480 UNIVERSITY ST., MONTRÉAL (QUÉBEC) H3A 2A7, CANADA,

E-mail address: steph@cim.mcgill.ca

Typeset by $\mathcal{A}\mathcal{M}\mathcal{S}$-LaTeX